

# The self-exciting nature of the bid-ask spread dynamics

Ruihua RUAN<sup>\*1</sup>, Emmanuel BACRY<sup>1</sup> and Jean-François MUZY<sup>2</sup>

<sup>1</sup>CEREMADE, CNRS-UMR 7534, Université Paris-Dauphine PSL  
Place du Maréchal de Lattre de Tassigny, 75016 Paris, France

<sup>2</sup>SPE CNRS-UMR 6134, Université de Corse BP 52, 20250 Corte, France

June 7, 2023

## Abstract

The bid-ask spread, which is defined by the difference between the best selling price and the best buying price in a Limit Order Book at a given time, is a crucial factor in the analysis of financial securities. In this study, we propose a "State-dependent Spread Hawkes model" (SDSH) that accounts for various spread jump sizes and incorporates the impact of the current spread state on its intensity functions. We apply this model to the high-frequency data from the Cac40 Euronext market and capture several statistical properties, such as the spread distributions, inter-event time distributions, and spread autocorrelation functions. We illustrate the ability of the SDSH model to forecast spread values at short-term horizons.

**Keywords**— Spread dynamic, Hawkes process, High-frequency data, Market microstructure, Ergodic Markov process

## 1 Introduction

The bid-ask spread, defined at a given time in a Limit Order Book by the difference between the smallest ask (selling) price and the largest bid (buying) price, is a quantity of great interest for financial securities. It corresponds to the cost of an "immediate" transaction as respect to a more patient one. Many studies in economics literature are devoted to the bid-ask spread which is, in general, decomposed into order processing costs, adverse selection costs and inventory risk (for the liquidity providers/market makers who earn money from the spread) [Glosten and Harris, 1988, Stoll, 1989, Huang and Stoll, 1997, Glosten and Milgrom, 1985]. The spread is often used as a proxy for market liquidity a small spread being associated with very liquid markets. For a literature review of liquidity measures, we refer the reader to [Díaz and Escribano, 2020, Goyenko et al., 2009, Fong et al., 2017, Fosset et al., 2020b]. Let us also mention that the bid-ask spread has been proved to be very closely related to realized volatility. Indeed, many empirical studies [Goyenko et al., 2009, Fong et al., 2017] tend to prove that these two quantities are highly positively correlated [Bessembinder, 1994, Zumbach, 2004, Wyart et al., 2008, Dayri and Rosenbaum, 2015]. Many other statistical properties of the bid-ask spread have been the focus of various works. For instance, it has been shown that spread has a distribution that is fat-tailed and its dynamics is characterized by a long range (power-law) auto-correlation function [Mike and Farmer, 2008, Plerou et al., 2005,

---

<sup>\*</sup>Corresponding author. Email: ruan@ceremade.dauphine.fr

Bouchaud et al., 2018, Bouchaud et al., 2009, Groß-Klußmann and Hautsch, 2013, Fall et al., 2021]. In refs [Mike and Farmer, 2008, Ponzi et al., 2006, Zawadowski et al., 2006], it is shown that after a large variation of the spread (i.e., a temporary liquidity crisis), the spread decays slowly back to an equilibrium value. Let us note that, though, most of the time, these statistical properties are obtained through direct empirical studies on historical spread time-series, some papers tackle the statistical properties of the spread (mainly the distribution of the spread values) via some statistical models of the limit and market order flows [Bouchaud et al., 2002, Daniels et al., 2003, Smith et al., 2003, Foucault et al., 2005, Roşu, 2009, Abergel and Jedidi, 2013, Muni Toke and Yoshida, 2017]. The reader will find a good overview of the different statistical properties of the bid-ask spread in the chapter 7 of [Bouchaud et al., 2009].

In order to understand the properties of market prices and their formation, in the context of electronic markets, many approaches involving point processes have been proposed to describe the occurrence of order book events (see e.g. [Smith et al., 2003, Cont et al., 2010, Abergel and Jedidi, 2013]). Within this context, as reviewed in [Bacry et al., 2015], Hawkes processes is a very popular class of models that has proven very efficient to describe the dynamical properties of different quantities like the market activity [Bowser, 2007, Muni Toke and Pomponio, 2012, Hardiman et al., 2013, Morariu-Patrichi and Pakkanen, 2018], the mid-price [Bacry et al., 2013], the best bid / best ask prices [Lee and Seo, 2022] or the first (L1) book levels [Large, 2007, Bacry et al., 2016, Zheng et al., 2014]. Hawkes processes constitute a class of multivariate point processes that were introduced in the seventies by A.G. Hawkes [Hawkes, 1971] notably to model the occurrence of seismic events. They involve an intensity vector that is (in its original form) a simple linear function of past events. This popularity of Hawkes processes can be explained above all by their great simplicity and flexibility. Our main purpose in this paper is to study whether one can design a dynamical model for spread fluctuations based on Hawkes processes. Though many studies can be found in the literature about the bid-ask spread and its statistical properties, very few offer models for its high-frequency dynamics. Besides, some recent econometric approaches involving long-memory auto-regressive, Poisson point processes [Groß-Klußmann and Hautsch, 2013, Cattivelli and Pirino, 2019], one can mention few models that rely on Hawkes processes. In 2014, Zheng *et al.* proposed in [Zheng et al., 2014] one of the first model for the bid-ask spread dynamics of a financial asset. It uses a constrained 2-dimensional Hawkes process. The spread  $S_t$  is seen as a strictly positive integer value (a multiple of the tick value, i.e., the minimum increment defined by the market between two quotation values). The first (resp. second) dimension of this Hawkes process  $S_t^+$  (resp.  $S_t^-$ ) is used for coding the positive (resp. negative) jumps of the spread, it is an increasing function of time that jumps by 1 whenever a positive jump of the spread occurs. In this model all the jumps of the spread are considered to be of size 1 tick. Thus, one gets  $S_t = S_t^+ - S_t^-$ . The constrained Hawkes process is thus defined by the following expression of the intensity  $\lambda^+$  (resp.  $\lambda^-$ ) of the jump process  $S_t^+$  (resp.  $S_t^-$ ):

$$\begin{aligned}\lambda_t^+ &= \mu^+ + \sum_{e \in \{+, -\}} \int_0^t \phi^{+,e}(t-s) dS_s^e \\ \lambda_t^- &= 1_{S_{t-} \geq 2} (\mu^- + \sum_{e \in \{+, -\}} \int_0^t \phi^{-,e}(t-s) dS_s^e)\end{aligned}\tag{1}$$

where  $\mu^+$  (resp.  $\mu^-$ ) corresponds to a constant exogenous intensity (a term that does not depend on the past events) and the 4 functions  $\{\phi^{e,e'}(t)\}_{e,e'=\pm}$  are kernel causal (i.e., support in  $[0, +\infty[$ ) functions that encode the (endogenous) influence of past jumps (of type  $e'$ ) on the occurrence of future jumps (of type  $e$ ). Let us point out that for estimation purpose, the kernels are often taken to be exponential functions (or sum of exponential functions). Indeed, for such functions the likelihood is explicit and can be computed in a fast way. In [Zheng et al., 2014], simple exponential kernels were chosen :  $\phi^{e,e'}(t) = \alpha^{e,e'} \beta e^{-\beta t}$  ( $\beta$  is the same for all the kernels). Let us point out that, Zheng *et al.* introduced a non-linearity (the term  $1_{S_{t-} \geq 2}$ ) in the "classical" definition of a Hawkes process. This non-linearity is necessary to constrain the spread to keep from taking negative or zero values. In their work, Zheng *et al.* performed numerical estimation of their model (using Maximal Likelihood Estimations) and studied some statistical properties of their model. In a more recent paper [Fosset et al., 2020a], the authors build a simplified version of the previous model and focus on the relation between spread dynamics and liquidity crises. They introduce the constrained

2-dimensional Hawkes process defined by

$$\begin{aligned}\lambda_t^+ &= \mu^+ + \int_0^t \alpha \beta e^{-\beta(t-s)} dS_s^+ \\ \lambda_t^- &= \mu^- 1_{\{S_t \geq 2\}}\end{aligned}\tag{2}$$

where the notations are exactly the same as in model (1). They use  $\alpha_c = 1 - \frac{\mu^+}{\mu^-}$  to distinguish different regimes. When  $\alpha < \alpha_c$ , the Hawkes system is stable and the invariant distribution of spread is given. When  $\alpha_c < \alpha < 1$ , the model is still stable but the spread has a linear growth. When  $\alpha > 1$ , the system is explosive and there is a liquidity crisis.

In this paper we propose an approach which is inspired by these two papers but that will focus more on fitting empirical features and matching observed properties from market data. More specifically, we propose a new ‘‘State Dependent Spread Hawkes’’ (SDSH) model in order to account for the bid-ask spread fluctuations. Our model can be seen as a generalization of the two previously introduced models in the sense that it is a  $2K$ -variate ( $K$  possibly greater than 1) Hawkes process that is able to account for the different jump sizes (up to size  $K$ ). It includes enough kernels to encode the influence of the various past jumps on the various future jumps. Each component includes a non-linearity component, as in the previous models, in order to ensure strictly positive values for the spread. In order to allow more complex dynamics, each kernel is written as a sum of several exponential functions (and not only one, as in the previous models). Our ambition is to capture all the aspects of the dynamics of the bid-ask spread that were not captured by the previous models.

The paper is organized as follows. The next section (Section 2) is devoted to a detailed definition of our new model for the bid-ask spread. The Markov and ergodicity properties of this model is studied in a particular case. Section 3 illustrates this model with some numerical simulations and presents the estimation procedure on these simulations. Section 4, the core of our paper, is devoted to empirical results. This section is divided in 4 subsections. The first two ones correspond to a quick presentation and basic statistical properties of the real financial time-series that will be used all along the section. The third one is devoted to estimation of our model on these data. Parameters estimation (including the kernels and the constraint parameters) are discussed thoroughly. The last one is devoted to the goodness of fit of the model through different quantities, mainly : the inter-event time distribution, the spread distribution and the autocorrelation function. Section 5 provides a first approach that demonstrates the interest of the SDSH model in the issue of short-term forecasting of spread values. We conclude in section 6.

## 2 Modeling spread dynamics using State Dependent Spread Hawkes processes

### 2.1 Notations

Let us consider a limit order book (LOB) associated with a given asset. We note  $S_t$  the bid-ask spread of this order book at time  $t$ , i.e., the difference, at time  $t$ , of the best ask price and the best bid price. We choose to express  $S_t$  in *tick* units (the *tick* corresponds to the smallest price increment authorized by the market).  $S_t$  is therefore a right continuous process that can take only integer (strictly positive) values (i.e.,  $S_t \in \mathbb{N}^*$ ). Its smallest possible value is  $S_t = 1$  (tick).

The process  $S_t$  can be seen as a jump process and various orders sent to the LOB, depending on their type and size may induce jumps on  $S_t$  of various sizes. In our model, an event corresponds to a jump of  $S_t$  of a given size. In practice, very large jumps almost never occur, so with no loss of generality, we can limit the set of events to  $\mathcal{E} = \{+1, +2, \dots, +K, -1, -2, \dots, -K\}$  (where  $K$  is a hyper parameter of the model to be fixed for each asset).

For each event  $e \in \mathcal{E}$  (i.e., for each jump size  $e$ ), we denote by  $S_t^e$  the counting process that counts (along

time, starting arbitrarily, at time 0) the number of jumps of size  $e$  that occurs. Thus, the spread process  $S_t$  can be written as:

$$S_t = S_0 + \sum_{k=1,2,\dots,K} kS_t^{+k} - \sum_{k=1,2,\dots,K} kS_t^{-k}. \quad (3)$$

In real limit order books, it is clear that the dynamics of the spread jumps highly depend on the size of the jumps, it is thus natural to build a model that allows different dynamics for different jump sizes.

## 2.2 The SDSH spread model

Our model for spread dynamics basically consists in considering that the multivariate counting process  $\{S_t^e\}_{e \in \mathcal{E}}$  follows a  $2K$ -variate Hawkes process. However, since the dynamics of the various events depend on the state of the current spread  $S_t$  itself (the least being that when the spread is 1 tick, no negative event can occur), we introduce, in the classical Hawkes framework, a term that depends on  $S_t$ , i.e., a *state variable* that accounts for the current size of the spread. More precisely, if we note  $\lambda_t^e$  the conditional intensity (at time  $t$ ) of the counting process  $S_t^e$ , the State Dependent Spread Hawkes spread model writes:

$$\lambda_t^e = f^e(S_{t-}) \left[ \mu^e + \sum_{e' \in \mathcal{E}} \int_0^t \phi^{e,e'}(t-s) dS_s^{e'} \right] \quad (4)$$

where (following the classical Hawkes processes framework)

- $\mu^e$  is the exogenous base intensity for the jumps of size  $e$
- $\Phi(t) = \{\phi^{e,e'}(t)\}_{e,e' \in \mathcal{E}}$  is the Hawkes kernel matrix whose elements are the Hawkes (positive valued) interaction kernels, encoding the influence of past jumps of size  $e'$  on future jumps of size  $e$ .
- we assume that these kernels are parameterized as a sum  $L$  exponentials, i.e.,

$$\phi^{e,e'}(t) = \sum_l^L \alpha_l^{e,e'} \beta_l e^{-\beta_l t}, \quad (5)$$

(this is hardly restrictive since many behaviour can be easily reproduced by a sum of exponentials [[Bochud and Challet, 2007](#)])

and where the current size of the spread is taken into account through the global multiplicative term  $f^e(S_{t-})$  where

- $S_{t-}$  is the the left limit of  $S$  at time  $t$  (i.e., the spread size "just before" time  $t$ ),
- $f^e$  is a non-negative function defined on  $\mathbb{N}^*$ , with the constraint that  $f^{-k}(n) = 0$  when  $n - k \leq 0$  (in order to prevent jumps that would lead to a non strictly positive value for the spread). Let us note that the Equation (5) does not change if we multiply  $f^e$  by a factor and divide  $\mu^e$  and the  $\phi^{e,e'}$  by the same factor. So, in the following, we will fix arbitrarily the first non zero value of  $f^e(s)$  to be 1, i.e.,  $f^e(\min_s \{s, f^e(s) \neq 0\}) = 1$ .

Let us point out that, in order to account for the impact of the current spread size on the different dynamics of the spread jumps, several choices could have been made. Maybe, the most natural one would have been to make the kernel themselves depend on the spread size  $S_{t-}$ . However, such a choice would lead to increase drastically the number of parameters needed to encode the kernels themselves, leading to important estimation instabilities. The choice we made allows several things at once

- keeping the number of estimation parameters low
- encoding in an easy way the fact that negative values for  $S_t$  are not allowed

- allowing the model to account for the well known fact that the spread dynamics is mainly mean reversing and, the higher the spread size is, the higher is the probability for large negative jumps to occur.

## 2.3 Markov property and ergodicity

Using Eq. (3), it is easy to prove that, since the Hawkes kernels are sums of exponential functions, then the following property holds:

**Proposition 1.** *The process  $(S_t, X_t)$ , where  $X_t^{e,e'} := \int_0^t \phi^{e,e'}(t-s) dS_s^{e'}$ , is a Markov process*

In the simple case where  $K = 1$  (i.e., only jumps of size +1 or -1 are allowed) and  $L = 1$  (i.e., only one exponential kernel), one can prove (see Annex A) the following ergodic property :

**Proposition 2.** *Assume  $K = 1$ , i.e.,  $\mathcal{E} = \{-1, 1\}$  and  $L = 1$ , i.e.,  $\phi_{e,e'}(t) = \alpha^{e,e'} \beta e^{-\beta t}$ , If the following conditions are satisfied :*

$$(A) = \begin{cases} f^-(1) = 0 & (A_1) \\ f^-(S) \geq \gamma S \text{ for some } \gamma > 0 \text{ when } S \geq 2 & (A_2) \\ \sup_{S \geq 1} \{f^+(S)\} (\alpha^{+,-} + \alpha^{+,+}) < 1 & (A_3) \end{cases}$$

then the process  $(S_t, X_t)$  is a  $V$ -uniformly ergodic Markov process.

Thus, under these assumptions, the spread process has some stationary distributions. Let us notice that condition (A<sub>2</sub>) is a condition ensuring a "return to the mean value" analog to the condition of a proportional cancellation rate in [Smith et al., 2003, Abergel and Jedidi, 2013, Wu et al., 2019]. The condition (A<sub>3</sub>) corresponds to a stability condition ensuring that the number of upward spread jumps does not diverge exponentially in a finite interval. This is a first result, the general proof (for any  $K$  and  $L$ ) seems to be much more difficult (see Remark 3), it will be the focus of a forthcoming paper.

## 3 Numerical simulation of the SDSH spread model and parametric estimation

### 3.1 Simulation

In order to perform numerical simulations, we use the classical "thinning method" introduced by [Lewis and Shedler, 1979, Ogata, 1981] and implemented in the *tick* open source library [Bacry et al., 2017].

To make it easier for readers to understand how our model works in practice, Figure 1 shows the result of such a simulation during the first 20 seconds. We chose the following parameters

- $K = 1$ , i.e.,  $\mathcal{E} = \{+1, -1\} =: \{+, -\}$
- $L = 1$  and  $\phi^{e,e'}(t) = \alpha^{e,e'} e^{-\beta t}$ , where  $\beta = 1$ ,  $\alpha^{+,+} = \alpha^{-,-} = 0.1$  and  $\alpha^{+,-} = \alpha^{-,+} = 0.2$
- $\mu^+ = \mu^- = 0.3$
- $f^+(1) = 1, f^+(2) = 0.7$  and  $f^+(S) = 0.3$  for  $S \geq 3$ ,
- $f^-(1) = 0, f^-(2) = 1$ , and  $f^-(S) = 5$  for  $S \geq 3$ .

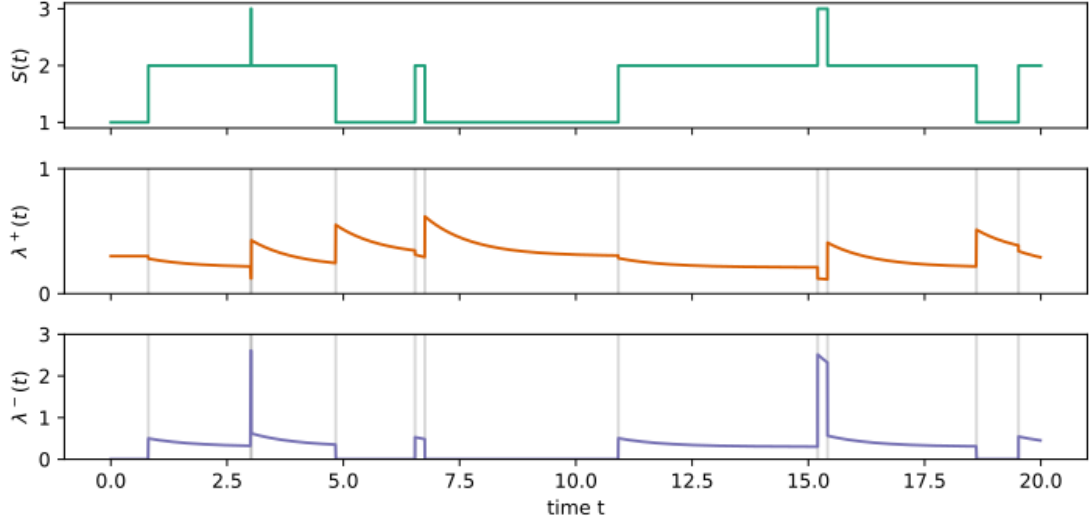


Figure 1: A realization of the SDSH spread model during 20 seconds using parameters as indicated in the text. As we see, since we chose  $f^-(S)$  to be very large (5) as soon as  $S \geq 3$ , the spread does not stay long at a value of 3.

### 3.2 Estimation principles

For parametric estimation, we will use again the *tick* python open source library which natively allows robust parametric Maximum Likelihood Estimation (MLE) estimation of multi-dimensional Hawkes processes using sum of exponentials. We slightly tweaked the algorithms of this library in order to take into account the  $f^e(S)$  terms. The algorithm used in this model closely follows the one used for the QRH-II model described in [Wu et al., 2019]. The likelihood function for this model is located in Appendix B.

More precisely, prior to the parametric simulation, a certain number of hyper-parameters have to be fixed (according to the specificity of the corresponding assets, see Section 4 for specific cases) :

- $K$  : the highest jump size allowed by the model. This hyper-parameter should be carefully chosen after looking at the effective probability of occurrence of various jump sizes on the real data,
- $L$  and  $\{\beta_l\}_{l \in L}$  : in practice choosing the  $\beta_l$  so that they are logarithmically spaced is sufficient to recover a very large variety of behavior, i.e.,  $\beta_l = \beta_1 10^{l-1}$ .  $L$  and  $\beta_1$  should be chosen to adapt to the timescale range one is interested in.
- each  $f^e(s)$  is a function of  $s \in \mathbb{N}^*$ , thus corresponds to an infinite number of parameters. For parametric estimation to be feasible, we have somehow to make some assumptions on the behavior of the  $f^e(s)$  functions for large  $s$ . Very large spread are extremely rare events, so basically any assumption will work, as long as it enforces mean reversion of the spread. Thus, we arbitrarily chose to consider that all the functions  $f^e(s)$  are constant for  $s$  greater than a fixed value  $\bar{S}$ . In practice, the value of  $\bar{S}$  should be chosen so that spread of size greater than  $\bar{S}$  should be extremely rare events.

Given these hyper-parameters, our MLE parametric estimation algorithm allows to estimate

- the exogenous intensities  $\{\mu^e\}_{e \in \mathcal{E}}$  (so a total of  $2K$  parameters)
- the kernel parameters  $\{\alpha_l^{e,e'}\}_{l \in L, (e,e') \in \mathcal{E}^2}$  (so a total of  $4LK^2$  parameters)
- the values  $\{f^e(s)\}_{e \in \mathcal{E}, s \in [1.. \bar{S}]}$  (so a total of  $(2K\bar{S} - \frac{K^2+K}{2} - 2K)$  parameters, as long as  $K < \bar{S}$  (let us remind that we fixed arbitrarily the first non zero value of  $f^e(s)$  to be 1.)

So that amounts to  $2K + 4LK^2 + 2K\bar{S} - \frac{K^2+K}{2} - 2K$  parameters.

In the following we illustrate the estimation procedure on simulated data.

### 3.3 Estimation on simulated data

In this example, we simulated our model in dimension 2, i.e., for  $\mathcal{E} = \{+1, -1\} := \{+, -\}$ : the only possible moves for the spread are upward or downward moves of one tick. Simulation (using the thinning method [Lewis and Shedler, 1979, Ogata, 1981] as explained in Section 3.1) was run to produce 50 samples of size 5000 seconds using the following parameters. We set the parameters for the simulation to be (using the notations introduced in Section 2.2) :

- $\mu^+ = 0.3, \mu^- = 0.2$
- $L = 2$  with  $\beta_1 = 20s^{-1}, \beta_2 = 200s^{-1}$  and the Hawkes kernel is

$$\phi(t) = \begin{pmatrix} 2 & 6 \\ 10 & 0 \end{pmatrix} e^{-20t} + \begin{pmatrix} 4 & 20 \\ 20 & 4 \end{pmatrix} e^{-200t}$$

- $f^+(1) = 1, f^+(2) = 0.8, f^+(3) = 0.5, f^+(s) = 0.2$  for  $s \geq 4$   
 $f^-(1) = 0, f^-(2) = 1, f^-(3) = 2, f^-(s) = 3$  for  $s \geq 4$

**Estimation** Then we estimate the parameters using  $\beta_1 = 10s^{-1}, \beta_2 = 100s^{-1}, \beta_3 = 1000s^{-1}$ , i.e.

$$\phi(t) = 10 \begin{pmatrix} \alpha_1^{++} & \alpha_1^{-+} \\ \alpha_1^{+-} & \alpha_1^{--} \end{pmatrix} e^{-10t} + 100 \begin{pmatrix} \alpha_2^{++} & \alpha_2^{-+} \\ \alpha_2^{+-} & \alpha_2^{--} \end{pmatrix} e^{-100t} + 1000 \begin{pmatrix} \alpha_3^{++} & \alpha_3^{-+} \\ \alpha_3^{+-} & \alpha_3^{--} \end{pmatrix} e^{-1000t}$$

As it can be seen in Fig. 2, our estimation method allows one to recover the parameter values  $\mu^e$  and to reproduce very well both the functions  $f^e(S)$  and the Hawkes kernel shapes. It is worth noting that the basis exponential functions for the simulation are very different from those for estimation.

## 4 Empirical results

### 4.1 Data

In this section, we calibrate the SDSH spread model using high-frequency data from the Cac40 french Euronext Market. The data correspond to every single change of the spread (characterized by the size of the change and a time stamp with a precision of  $1\mu s$ ) for 3 stocks, namely AXA, BNP and NOKIA and for the CAC40 index Future. The data for stocks (resp. Cac40 Future) are extracted from February 1st 2017 (resp. January 4th 2016) to February 28th 2018 (resp. February 28th 2017). In order to minimize the intraday seasonality of the data we used only the data in the intraday slot [10am,12am]. Thus, for a given asset, the estimation of the model will be performed considering each day as an independent realization. Thus, in order to avoid days with too short time series, we took out, for a given asset, all the days associated with a number of events (i.e., spread changes) below a threshold. We refer the reader to the Table 1 for getting some basic information on each of these data series. Let us point out that the Cac40 Future has a much larger tick size than the 3 other assets, we expect the jump size for the spread to be much smaller on average.

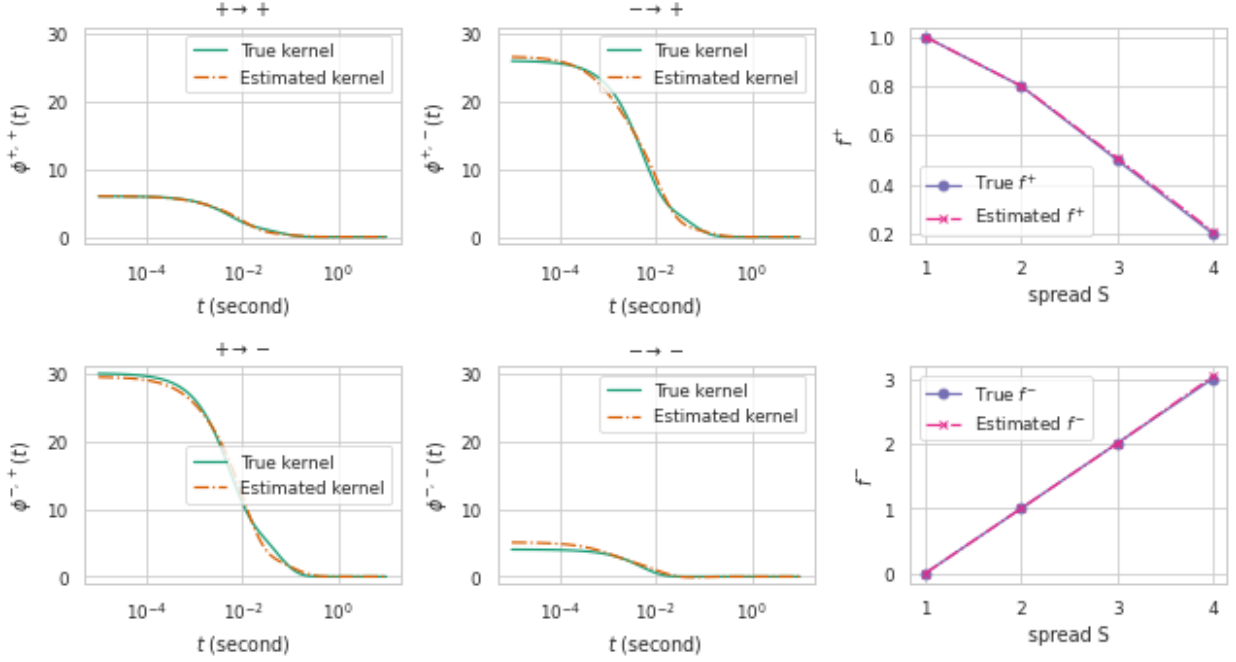


Figure 2: Numerical estimation from samples of a SDSH spread model. The 4 figures on the left show the true kernels and the estimated kernels, and the 2 figures on the right show the true  $f$  values and the estimated  $f$  values. The estimated  $\mu^+$  is 0.29 and the estimated  $\mu^-$  is 0.19.

Asset	tick size	Min. #events	#days	Total #events	$\mathbb{E}_{event}[S]$	$\mathbb{E}_{cal}[S]$
CAC40 Future	0.5	5,000	100	1,026,156	1.51	1.40
AXA	0.005	3,000	130	617,309	2.44	3.04
BNP	0.01	5,500	100	1,079,464	2.54	3.17
NOKIA	0.001	2,000	108	570,754	3.52	4.43

Table 1: Characteristics of the data used for model estimation. For each asset, for each day we only consider the slot [10am,12am]. Moreover, we keep only days where the number of events (i.e., the number of times the spread changes) is above the 'Min. #events' number.  $\mathbb{E}_{event}[S]$  and  $\mathbb{E}_{cal}[S]$  are the expectations of spread with two different distributions : event time distribution and calendar time distribution. See Eq. (7) and (6) for their definitions.

## 4.2 Spread distribution and hyper-parameter settings

In order to choose the the value for hyper parameters, following the lines of Section 3.2, we have to study the empirical distribution of the spread. Inspired by [Bouchaud et al., 2009], we can consider two ways to measure the spread distribution. They are both constructed by an average over daily distributions which can be obtained in two ways :

- Calendar time daily distribution :

$$\mathbb{P}_{cal}(spread = S) = \frac{1}{T} \int_0^T 1_{S_u=S} du \quad (6)$$



(where  $[0, T]$  corresponds to the slot 10am-12am)

- Event time daily distribution :

$$\mathbb{P}_{event}(spread = S) = \frac{1}{N} \sum_{n=1}^N 1_{[S_{t_n} = S]} \quad (7)$$

(where  $N$  is the total number of events on a given day).

The solid lines in Figure 12 illustrates the so-obtained results. Let us point out that it also displays (the right column) the distribution of the variation of the spread, i.e.,  $dS$ .

**Choice of  $K$ .** As expected, since the tick of the Cac40 Future is much larger than the other assets, we expect the values of the spread variations to be mainly of 1 tick. One can see that this is indeed that case in the last figure 12c: the amplitude of spread variations  $dS$  is never larger than 1 tick. Consequently, it seems natural to choose  $K = 1$  for this asset. If we follow the same guidelines (i.e., choosing the value of  $K$  as the minimum value so that the events corresponding to a change of the spread of  $K$  ticks is very rare) we see that choosing  $K = 2$  for all the other assets seems reasonable (see Figure 6, 12a, 12b).

**Choice of  $\bar{S}$ .** As explained in Section 3.2, choosing arbitrarily  $\bar{S}$  as the minimum value for which the probability of the spread to be this value is not extremely close to zero seems reasonable (there is no way we have enough information to perform reliable estimation of  $f^e(S)$  for values of  $S$  which hardly never occur). More precisely, we chose  $\bar{S}$  to be the maximum  $s$  for which  $\mathbb{P}_{event}(Spread = s) \geq 1\%$ . This leads to the following values :  $\bar{S} = 5$  (AXA),  $\bar{S} = 5$  (BNP),  $\bar{S} = 8$  (Nokia) and  $\bar{S} = 2$  (CAC40 Future).

**Choice of  $L$ .** As we will see (see Section 4.3.2), choosing  $L = 6$  and  $\beta_1 = 10^{-1}s^{-1}$  for all the assets (consequently, following Section 3.2  $\beta_2 = 1s^{-1}$ ,  $\beta_3 = 10s^{-1}$ ,  $\beta_4 = 10^2s^{-1}$ ,  $\beta_5 = 10^3s^{-1}$ ,  $\beta_6 = 10^4s^{-1}$ ) is sufficient to capture the kernels dynamics on the time-scale  $[10^{-4}s, 10s]$ . Let us point out that we performed estimation with largest values of  $L$  and smaller values of  $\beta_1$ , it does not change significantly the results (while it increases significantly the duration of the estimation procedure or alternatively leads to unstable results).

Table 3 summarizes all the choices for the hyper parameters

Asset	$K$	$\bar{S}$	Kernel time scale	# parameters
AXA	2	5	$10^{-4}s \rightarrow 10^1s$ ( $L = 6$ )	113
BNP	2	5	$10^{-4}s \rightarrow 10^1s$ ( $L = 6$ )	113
NOKIA	2	8	$10^{-4}s \rightarrow 10^1s$ ( $L = 6$ )	125
CAC40 Future	1	2	$10^{-4}s \rightarrow 10^1s$ ( $L = 6$ )	27

Table 2: Values chosen for the hyper parameters (following the guidelines in Section 3.2) for each dataset corresponding to each asset.  $K$  corresponds to the maximum jump size for the spread.  $\bar{S}$  to the abscissa above which the functions  $f^e(s)$  are considered as constant and the Kernel time scales is deduced from the choice of  $L$  and  $\beta_1$

### 4.3 Estimation

We performed parameters estimation on each time-series described in the previous Section using MLE following the guidelines of Section 3.2. As explained in this Section, all the estimations in this paper were performed using the *Tick* open-source package [Bacry et al., 2017], after having adapted the MLE exponential-kernel estimation algorithm of *Tick* to account the state dependent function  $f^e(S)$ . In the following we will show the various results of this estimation and comment on them, starting with the estimation of the  $\{f^e(s)\}_{e \in \mathcal{E}}$  functions and then of the kernels  $\{\phi^{e,e'}(t)\}_{e,e' \in \mathcal{E}}$  themselves.

#### 4.3.1 Estimation of the $\{f^e(s)\}_{e \in \mathcal{E}}$ functions

The results of the estimation procedures for the different assets are reported on Fig. 3 (let us recall that, for each  $e$ , the first positive value of  $f^e(S)$  is arbitrarily set to 1).

We first remark that all estimated curves display the same behavior for all assets. As expected, we see that the  $f^e$  functions corresponding to positive events (i.e., upward jumps,  $e \in \{+1, +2\}$ ) are decreasing functions that decrease pretty quickly towards a value close to 0 whereas the  $f^e$  functions corresponding to negative events (i.e., downward jumps,  $e \in \{-1, -2\}$ ) are rapidly increasing functions. When the spread is high, it is clearly pressed downward by inhibiting the positive events (with small  $f^{+1}(s)$  and  $f^{+2}(s)$  for large spread), and by exciting the negative events (with large  $f^{-1}(s)$  and  $f^{-2}(s)$  values).

The two functions  $f^{-1}$  and  $f^{-2}$  are clearly saturating though saturation seems to appear faster on  $f^{-1}$  than on  $f^{-2}$ . Let us recall that one cannot perform estimation for larger spread than the chosen  $\bar{S}$  due to the lack of statistics (i.e., spread values above the chosen  $\bar{S}$  are extremely rare events).

Let us remark that, as expected, the so-obtained range for the values of the function corresponding to negative events is in line with the corresponding tick size (and the average spread size) of each asset (see Table 1). Indeed, the largest the tick size (the smallest the average spread) the smallest the range of values : going from CAC40 Future (being the largest tick size) to NOKIA (being the smallest tick size).

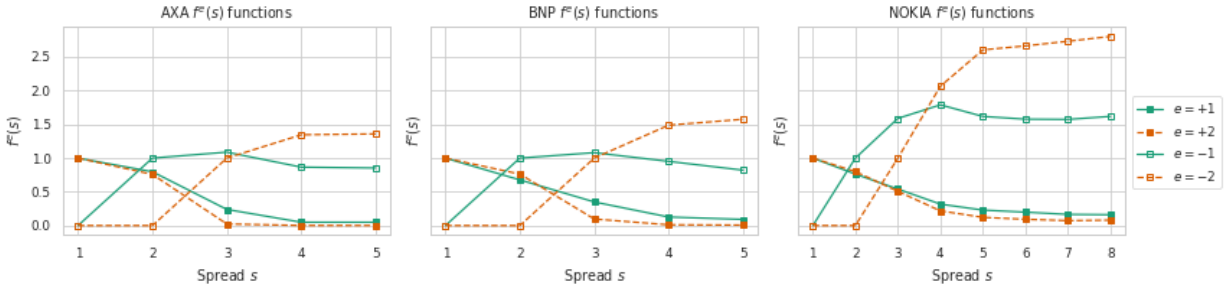


Figure 3: Estimations of the  $\{f^e(s)\}_{e \in \mathcal{E}}$  functions for AXA (left), BNP (middle), NOKIA (right),  $\mathcal{E} = \{-2, -1, +1, +2\}$ . As for CAC40 Future, the  $\bar{S}$  is 2 and the  $K$  is 1, therefore  $f^{-1}(1) = 0$ ,  $f^{-1}(s) = 1$  if  $s \geq 2$ ,  $f^{+1}(1) = 1$ ,  $f^{+1}(s) = 0.0104$  if  $s \geq 2$ . For each  $e$ , the first positive value of  $f^e(S)$  is arbitrarily set to 1.

#### 4.3.2 Estimation of Hawkes kernels $\{\phi^{e,e'}(t)\}_{e,e' \in \mathcal{E}}$

First, let us point out that our estimation procedure essentially leads to positive valued kernels. Let us recall that the MLE procedure described in Section 3.2 is able to reveal inhibition behavior (i.e., significantly negative valued kernels) when present in the signal. Actually, if one zooms some of the kernels, one would reveal some negative values for a few kernels, but their absolute values are very small and not significant.

Of course, this does not mean that there is no inhibition behavior in the spread counting process. Actually the inhibition behavior are extremely strong but they are taken care, for each component  $S_t^e$ , by the multiplicative term  $f^e(S_{t-})$ . Recall, this is the main reason why we initially introduced them in our model ("hard" inhibition of some components to prevent negative spread values).

### Comparison of kernel integrated quantities

Let emphasize that, the introduction of multiplicative terms in the "State Dependent" Hawkes model (i.e., the fact that our model is not a plain vanilla Hawkes model due to the role of the state variable  $S_t$ ) keeps us from regular interpretations of the  $L^1$  norm of the Hawkes kernels. Indeed, in a vanilla Hawkes model, one generally compare the different values of the  $L^1$  norms  $\{\|\phi^{e,e'}(t)\|_1\}_{e,e' \in \mathcal{E}}$  and uses the classical populationnal interpretation of a Hawkes model ( $\|\phi^{e,e'}(t)\|_1$  represents the average number of events of type  $e'$  "directly" generated by an event of type  $e$ ) in order to disentangle the overall dynamics of the process. In our case, this interpretation is not possible. Not only it is conditioned to a spread value but the comparison between two norm values  $\|\phi^{e_1,e'}(t)\|_1$  and  $\|\phi^{e_2,e'}(t)\|_1$  for two different components  $e_1 \neq e_2$  does not make sense.

However, one can still compare the influence of all the past events of a given type  $e'$  on the occurrence of an event of a given type  $e$ . Indeed, given a spread jump of size  $e$  at time  $t_k$ . Thus, the spread jumps from the value  $s$  (at time  $t_k^-$ ) to  $s + e$  (at time  $t_k^+$ ), where  $s = S_{t_k^-}$ . Then one could study the influence of each endogenous term in the sum (within the brackets) in (4), thus comparing the relative values  $\int_0^{t_k^-} \phi^{e,e'}(t-s) dS_s^{e'}$  for different  $e'$  in order to understand which event type  $e'$  is influencing the most the occurrence at time  $t_k$  of the jump of size  $e$ . For that purpose, let us introduce the quantity

$$I_{s,e,t_k}(e') := \int_0^{t^*} \phi^{e,e'}(t^* - u) dN_u^{e'}, \quad \forall e'$$

for a jump of size  $e$  occurring at time  $t_k$  and leading to a spread value of  $s$ . We can then define the corresponding averaged values

$$\bar{I}_{s,e}(e') := \frac{\sum_{t_k: dS_{t_k}=e, S_{t_k^-}=s} I_{s,e,t_k}(e')}{\#\{t_k : dS_{t_k} = e, S_{t_k^-} = s\}}.$$

and finally the relative values

$$\tilde{I}_{s,e}(e') = \frac{\bar{I}_{s,e}(e')}{\sup_{e'} \bar{I}_{s,e}(e')} \quad (8)$$

Figure 10 displays this quantity for AXA, for each value of  $s$ , as an image (for which the vertical axis is  $e$  and the horizontal axis is  $e'$ )<sup>1</sup>. Readers are invited to refer to Appendix C Fig.10 for additional figures of the remaining stocks. These figures show what seems to be a universal feature for stocks : the occurrence of a jump of size  $e$  is essentially triggered by past occurrences of contrariant jump of size  $-e$ .

### Comparison of the kernel shapes

Finally, estimation results show that the most energetic kernels are decreasing "slowly", i.e., as a power-law  $t^{-\beta}$  with an exponent  $\beta \simeq 1$ . Such a power-law shape of the cross-excitation kernels is not surprising since this behavior with similar exponent values have been observed by various authors when modelling the market activity [Bacry et al., 2015] or the dynamics of mid-price [Bacry et al., 2016]. Figure 5 shows the contrariant kernels for the different stocks in a log-log plot. We see that they display a power-law behavior on 3 or 4 decades (depending on the kernel). (See Fig. 11a, 11b, 11c for the other assets in Appendix C.)

Moreover, most of them display a very clear bump around the time  $t \simeq 0.2ms$ . This is not very surprising, this phenomenon has already been revealed in several former works [Bacry et al., 2016, Rambaldi et al., 2017].

<sup>1</sup>Let us note that, since for CAC40, most of the time the spread is of size  $S = 1$  (the only other possible state is  $S = 2$  which happens very rarely), this type of analysis is not relevant

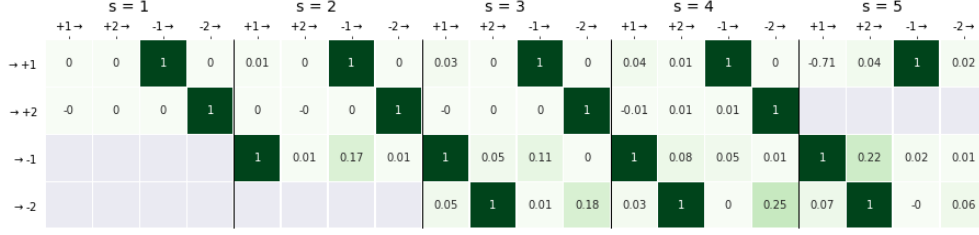


Figure 4: Relative kernel integrated quantities  $\tilde{I}_{s,e}(e')$  for AXA. For each stock, for each value of  $s$ , an image is displayed showing  $\tilde{I}_{s,e}(e')$  (defined by (8)) as a function of  $e$  (vertical axis) and  $e'$  (horizontal axis).

It corresponds to an average value of the latency of the market itself, i.e., the average time for an agent to effectively place an order, reacting to a change of the order book.

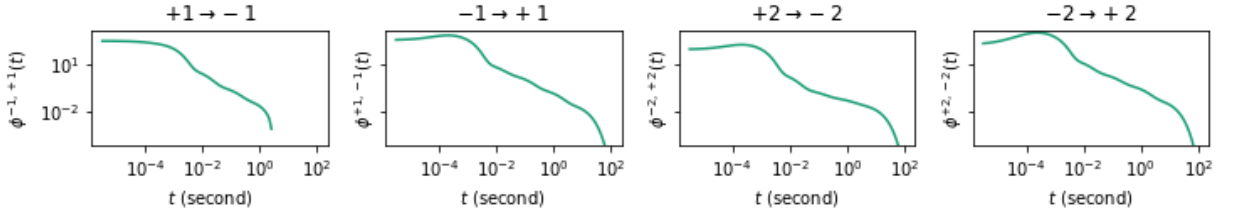


Figure 5: Hawkes kernels for AXA. In this figure we present four contrariant Hawkes kernels (i.e., with  $e$  and  $e'$  with different signs) . Each kernel  $\phi^{e,e'}$  (labeled  $e' \rightarrow e$  on the figure with  $e, e' \in \mathcal{E}$ ) represents the influence of the past jumps of size  $e'$  on the occurrence probability of a future jumps of size  $e$ . Each kernel is represented by a sum of  $L = 6$  exponentials, i.e.,  $\phi^{e,e'}(t)$ , where  $\phi^{e,e'}(t) = \sum_l^L \alpha_l^{e,e'} \beta_l e^{-\beta_l t}$ , where  $\beta_l = \frac{1}{\tau_l}$  with  $\tau_l$  taken in  $\{10^{-4}s, 10^{-3}s, \dots, 10^1s\}$  All the kernels are displayed on a log-log scale and show a power law behavior on a large range of scales (3, 4 or even 5 decades)

## 4.4 Goodness-of-fit

As we will show in this section, the model that we have built and estimated in the previous sections, is able to capture accurately very different statistical properties of the spread process. We will study successively, the spread distribution itself (that has already been discussed in Section 4.2), the inter-event-time distributions (i.e., time between change of spread values), the spread autocorrelation function and finally the auto-covariance function of the spread increment process.

### 4.4.1 Spread Distributions

Let us first compare the spread distributions obtained on true data (both calendar time and event time) that have been already discussed in Section 4.2 and the ones obtained with data simulated by our model (fitted on true data).

Following the same lines as in Section 4.2, Fig.6 displays both calendar-time spread distribution, event-time distribution and spread jumps ( $dS$ ) distribution for the AXA asset. We see that the model fits very precisely all these distributions. Several works have explored the distribution of spread, but [Fosset et al., 2020a] is one of the few that discuss it in detail. In their spread model (as shown in Equation (2)), the distribution

of spread is geometric, given by :

$$\mathbb{P}(S \geq n) = \frac{1 - \alpha_c}{1 - \alpha} (1 - r) r^{n-2} \quad \text{for } n \geq 2$$

where  $\alpha_c = 1 - \frac{\mu^+}{\mu^-}$  and  $r \in (0, 1)$  depends on  $\alpha$  and  $\beta$ . However, since  $\mathbb{P}(S = n)$  is a decreasing function for  $n \geq 2$ , the model Eq. (2) can only produce spread distributions that peak at  $S = 1$  or  $S = 2$ . As shown in Figure 6 and 12, this is not consistent with actual data.

It is also important to note that the SDSH model is not limited to reproducing the spread distribution, but is a more comprehensive framework which can capture a wider range of spread dynamics.

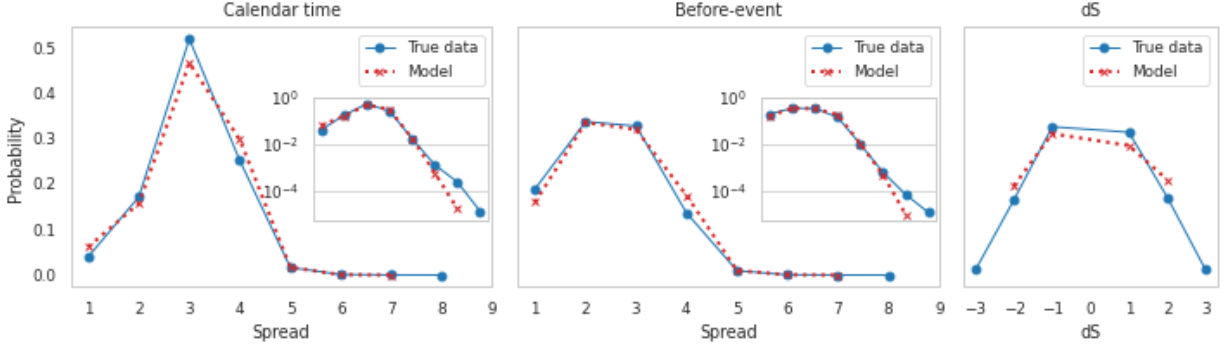


Figure 6: Spread distribution, comparison between true data and the the data obtained through simulation for AXA. The left-hand figure is the Calendar time distributions, the middle figure is the event time distributions, and the right-hand figure is the distributions of spread jumps size.

#### 4.4.2 Inter-event time distributions

Let  $\{t_n\}_n$  be the successive times the spread process  $S$  jumps (i.e., the spread changes). We define the inter-event-times  $\{\Delta t_n\}_n$  by

$$\Delta t_n = t_n - t_{n-1}.$$

The first plot on the left of Fig.7a displays the empirical unconditional distribution of the inter-event-times for both the AXA true data and some simulated data using our model (fitted with AXA data). The two other plots on the right hand-side of this latter plot show some conditional inter-event-time distributions. More precisely we define the set

$$\{\Delta t_{S_1 \rightarrow S_2}\} := \{\Delta t_i \mid S(t_i+) = S_1, S(t_{i+1}+) = S_2\}, \quad (9)$$

where  $S(t_i+)$  is the value of the spread immediately after the jump at time  $t_i$ . The plot of Fig.7a in the middle shows the distribution of  $\{\Delta t_{1 \rightarrow 3}\}$  whereas the one on the extreme right shows the distribution of  $\{\Delta t_{3 \rightarrow 2}\}$ .

We see that the model performs extremely well in reproducing the unconditional and conditional inter-event-time distributions. The plots in Fig.7b display the qq-plots of the true distributions versus the model distributions. Their linear behavior show how good the fit of the model is.

We invite the reader to look at the results obtained for BNP, NOKIA or CAC40 Future in Appendix C (Figure 13, 14 and 15).

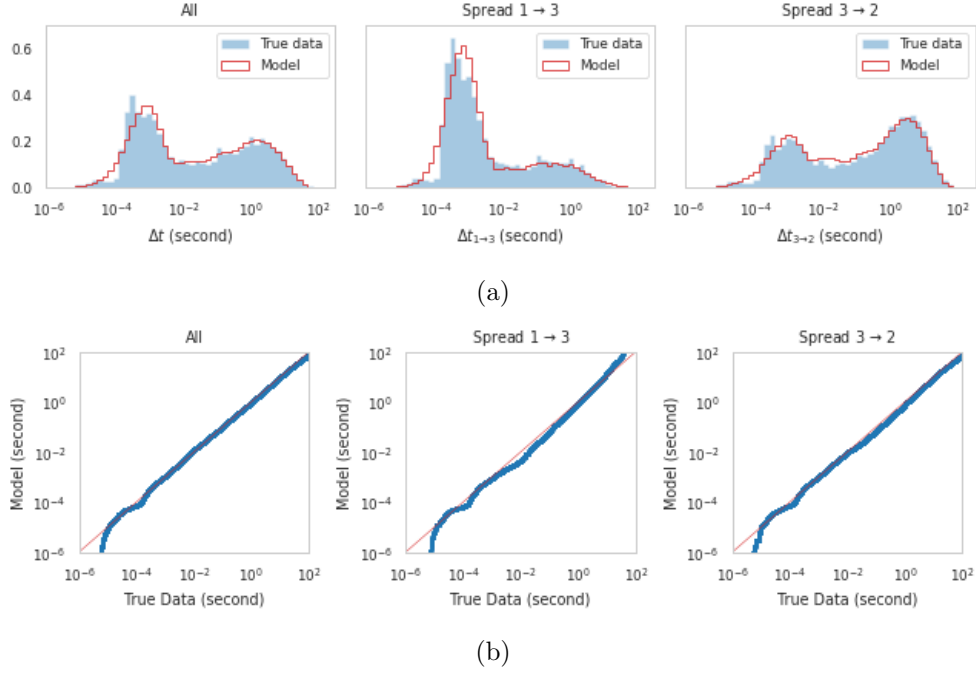


Figure 7: AXA Inter-event time unconditional and conditional distributions. Comparison between AXA true data and data obtained through simulation of our model (fitted on AXA data) (a) AXA true distributions versus model distributions for unconditional distribution or conditional distributions (see (9)). The x-axis is on log scale. (b) Corresponding qq-plots in log-log scales.

#### 4.4.3 Spread Autocorrelation

In this section, we study the auto-correlation function of the spread for true data and check in which respect the SDSH spread is able to faithfully reproduce it.

Estimation of the autocorrelation function of the spread on true data could a priori be done using straightforward quadratic covariations on all the available data. However such an estimation is likely to lead to some highly biased results. Indeed, it is well known that the orderbook dynamics (and consequently the spread dynamics) is subject to long range correlations and some very strong intraday seasonal effects [Bouchaud et al., 2009, Groß-KlußMann and Hautsch, 2013, Fall et al., 2021]. The seasonal effects must be taken care of in come ways in order to avoid these biases. One classical to do so is to limit the computation of the quadratic covariations so some limited time slot every day (assuming that the seasonal effects between the different days of the weeks are of second order). In our case, we used 15min time slots on the real data/ More precisely we used everyday the eight 15min slots between 10am and 12. As far as the model simulated data are concerned we used a single 2 hour time-slot (since there is no seasonality in the model, the length of the time slot is not important).

The plot of Fig.8 show these estimations for AXA (Additional plots for BNP, NOKIA and CAC40 are available in Appendix C Fig.16). On each plot the autocorrelation function for the true data and the autocorrelation function for the simulated data are shown, both in lin-lin scale and in log-log scale. Again the fits are amazingly good. The model succeeds in reproducing the autocorrelation function of the spread with a very good accuracy.

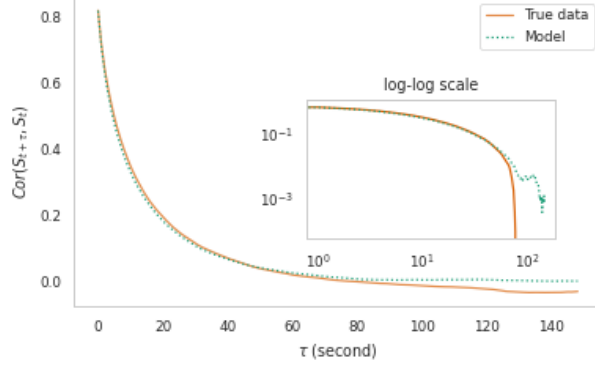


Figure 8: Auto-correlation function of the spread for AXA. True data versus model-simulated data. Each plot corresponds to a different asset. Quadratic variations were used for estimation. Eight 15min time-slots (between 10am and 12pm) were used everyday for true data in order to avoid intraday seasonal effects. 2 hours slots were used for model-simulated data.

#### 4.4.4 Autocovariance of spread increments

In this section we focus on the autocovariance function of the spread increments. Let us first define the exact quantity under study.

Let us define the infinitesimal covariance of the infinitesimal measure  $dS_t$ , namely  $Cov(dS_t, dS_{t'})$  which, assuming it is stationary, only depends on  $(t' - t)$ . Let us refer to it as  $g(t' - t)$ , i.e.,

$$\begin{aligned} g(t' - t)dt dt' &= Cov(dS_t, dS_{t'}) \\ &= \mathbf{E}[dS_t, dS_{t'}] - \mathbf{E}[dS_t]\mathbf{E}[dS_{t'}], \end{aligned}$$

Then, one gets,  $\forall \delta > 0$  and  $\forall \tau > 0$ ,

$$\begin{aligned} Cov(S_{t+\delta} - S_t, S_{t+\delta+\tau} - S_{t+\tau}) &= \mathbf{E}\left[\int_t^{t+\delta} dS_u \int_{t+\tau}^{t+\tau+\delta} dS_v\right] - \mathbf{E}\left[\int_t^{t+\delta} dS_u\right]\mathbf{E}\left[\int_{t+\tau}^{t+\tau+\delta} dS_v\right] \\ &= \int_t^{t+\delta} \int_{t+\tau}^{t+\tau+\delta} (\mathbf{E}[dS_u dS_v] - \mathbf{E}[dS_u]\mathbf{E}[dS_v]) \\ &= \int_t^{t+\delta} \int_{t+\tau}^{t+\tau+\delta} g(v - u) dudv \\ &= \delta^2 \int_0^1 \int_0^1 g(\tau + \delta(v - u)) dudv \end{aligned}$$

It is thus natural to introduce the normalized quantity (the relative covariance of spread increment during  $\delta$  seconds with lag  $\tau$  seconds)

$$ACV(\delta, \tau) := \frac{1}{\delta^2} Cov(S_{t+\delta} - S_t, S_{t+\delta+\tau} - S_{t+\tau}) \quad (10)$$

Let us point out that the function  $g(x)$  corresponds to the infinitesimal covariance function of a stationary process, it should thus decrease to 0 when the lag  $x$  goes to infinity. It seems reasonable to assume that it does so in a "regular way", i.e., that there exist  $\epsilon > 0$  and  $K > 0$  such that

$$|g'(x)| < Kx^{-\epsilon}, \quad \forall x > 0$$

Considering this assumption to be true, one gets, for any  $\tau > \delta > \delta' > 0$ , that

$$\begin{aligned}
|ACV(\delta, \tau) - ACV(\delta', \tau)| &= \left| \int_0^1 \int_0^1 (g(\tau + \delta(v - u)) - g(\tau + \delta'(v - u))) dudv \right| \\
&\leq (\delta - \delta') \max_{|y| \in [0, \max(\delta, \delta')]} |g'(\tau + y)| \int_0^1 \int_0^1 (v - u) \\
&\leq (\delta - \delta') \max_{|y| \in [0, \max(\delta, \delta')]} |g'(\tau + y)| \\
&\leq K \frac{(\delta - \delta')}{(\tau - \delta)^\epsilon}
\end{aligned}$$

Consequently, the covariance function  $ACV(\delta, \tau)$  can be estimated independently of the value of  $\delta$  as long as the lag  $\tau$  is large enough compared to the value of  $\delta$  that is being used. So in order to avoid having to perform estimation for all values of  $\delta$  and  $\tau$ , theoretically, one could fix a very small value for  $\delta$  and then estimate the ACV function on a range of  $\tau$  that satisfies  $\tau \gg \delta$ . However, as we will see, this will lead to very (high frequency) noisy estimations. In order to smooth out the estimation one needs to use a value for  $\delta$  that is much smaller than  $\tau$  but not "too" small.

Fig.9 not only illustrates this discussion but illustrates the fact that the model perfectly reproduces all the statistical features of the true data (of the AXA asset). The insert in the figure shows for a fixed  $\delta = 0.1s$  the function  $-ACV(\delta, \tau)$  as a function of  $\tau$  in a log-log scale. We chose to represent  $-ACV$  instead of  $ACV$  since, not surprisingly, due to the mean reversion property of the spread, we expect  $ACV$  to be mainly negative. One sees that if  $\delta$  is too small compared to  $\tau$  the result gets extremely noisy. Moreover one sees that the autocovariance function computed using the model simulated data reproduces very well the behavior of the one computed using the true data.

The main plot displays the different estimations of the  $ACV(\delta, \tau)$  as a function of  $\tau$  for different values of  $\delta$  (indicated on the legend on the right hand-side of the plot). Following what we just said, we limited for each  $\delta$  the estimation of  $ACV(\delta, \tau)$  for values of  $\tau$  on a range so that  $\delta$  is small compared to  $\tau$  but not too small. Doing so, we see that all the estimation curves fall "on top of the over", letting discover a smooth curve for the auto-covariance function on almost 7 decades of values for  $\tau$ . This curve is close to be linear indicating that the auto-covariance function is close to be power-law. One can see the slight latency bump around  $\tau = 200\mu s$  that was already pointed out in Section 4.3.2 when discussing Fig. 5 and 11. But what is really impressive is the way the estimation computed using the model-simulated data fits the estimation on true data on the whole range of scales. The fit is very accurate.

Last but not least, let us point out that one gets the exact same results when considering the other assets. This is illustrated in Fig. 17. Not only the model fits are extremely impressive but the auto-covariance curve look very much alike across the assets.

This seems to be the signature of what could be a stylized fact of the spread empirical processes

## 5 Illustration on using SDSH model for spread forecasting

The goal of this section is to show that the SDSH model is a good candidate to be used for high-frequency spread forecasting purposes. Spread forecasting is a difficult task that deserves a full paper dedicated on it with comparisons with state of the art methods. It is clearly out of the scope of our paper. In this section, we are far less ambitious and we just intend to give some very preliminary results that allow us to glimpse the possibilities of such an application.

The issue we consider is the prediction the spread value at a specific time horizon  $\Delta$  in the very near future (i.e.,  $\Delta < 1$  min). According to Fig. 9, a one-minute time window should be sufficient to capture the direct impact of past events on future spread values. Taking into account only the direct impact these events should be enough to capture most of the dynamics and to give a good idea of the order of the performance



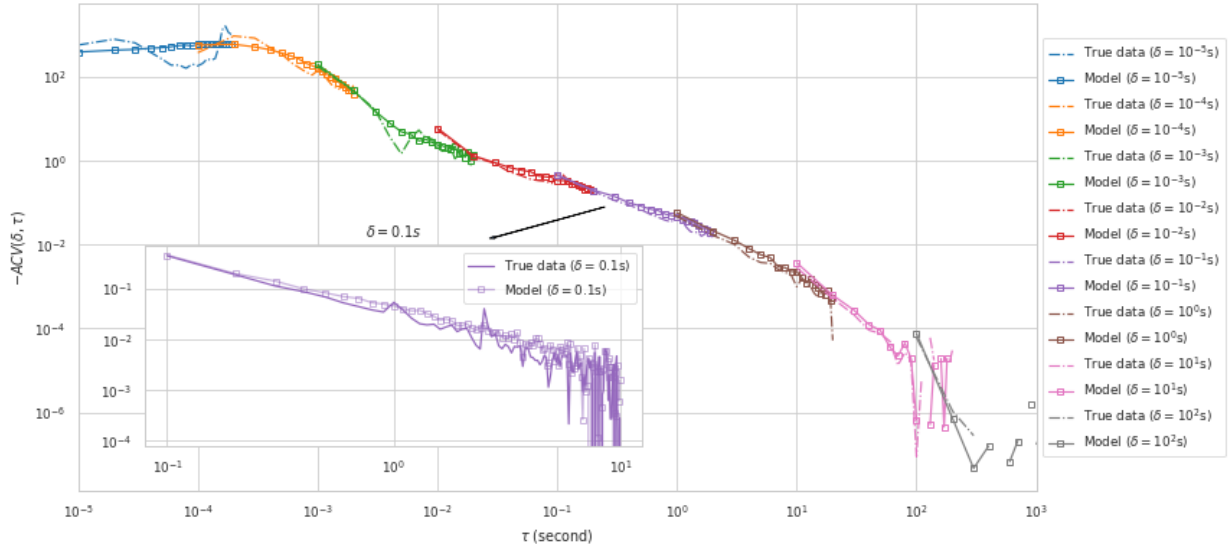


Figure 9: The  $-ACV(\delta, \tau)$  functions for different values of  $\delta$  as a function of  $\tau$  using a log-log scale both for using the AXA true data and the model-simulated data (fitted on AXA true data). As expected (see discussion) the curves for different  $\delta$ 's fall one onto the other letting discover a power-law behavior with a slight bump close to the latency time scale  $\simeq 200\mu s$  (see Section 4.3.2). The figure in the inset shows the particular curve  $ACV(\delta, \tau)$  for  $\delta = 0.1s$ . It clearly confirms the fact that if  $\tau$  is too far to  $\delta$  the estimation gets very noisy.

SDSH can reach. Since we don't have any explicit expression for the spread distribution, we rely on Monte Carlo simulations to estimate the expected spread value at the given time horizon. Let us be more precise.

At time  $t_0$ , the spread point process during the time interval  $[t_0 - 60, t_0]$  is sum up by  $\{S_u\}_{t_0-60 < u < t_0}$  or alternatively by  $S_{t_0-60}$  and all the events  $\{(t_i, e_i), t_0 - 60 \leq t_i < t_0\}_{i=1, \dots, n}$  that occur within the time-interval  $[t_0 - 60, t_0]$ . Thus, in order to estimate  $\mathbb{E}[S_{t_0+\Delta} | S_{u, u \in [t_0-60, t_0]}]$ , i.e., the conditional mean at time-horizon  $\Delta$ , we simulate 100 processes from  $t_0$  to  $t_0 + \Delta$  with the intensity function at time  $t \in [t_0, t_0 + \Delta]$  defined as

$$\lambda_t^e = f^e(S_{t-}) (\tilde{\mu}^e(t) + \sum_{e' \in \mathcal{E}} \int_{t_0}^t \phi^{e, e'}(t-u) dS_u^{e'}) \quad (11)$$

where the baseline  $\tilde{\mu}^e(t)$  is a function on  $t \in [t_0, t_0 + \Delta]$  defined by

$$\tilde{\mu}^e(t) = \mu^e + \sum_{e' \in \mathcal{E}} \sum_{i=1}^n 1_{e_i=e'} \phi^{e, e'}(t-t_i). \quad (12)$$

Before illustrating the performance of such an estimator, let us briefly describe an alternative model, previously introduced in [Groß-Klußmann and Hautsch, 2013], that we will use as a benchmark for our numerical tests.

**Introducing a benchmark: the Autoregressive Conditional Double Poisson (ACDP) model** In [Groß-Klußmann and Hautsch, 2013], the authors introduce various spread prediction models which are all based on the use of autoregressive conditional Poisson model. As our focus is on high-frequency prediction, we will consider only the so-called ACDP model and not its long-memory version (i.e., the LMACP, the Long Memory Autoregressive Conditional Poisson model). Again, let us point out that building an optimized SDSH-based forecast procedure and comparing it with the main state of the art procedures is out of the scope of this paper. A forthcoming work will be specifically dedicated to these issues.

Within the ACDP framework, the spread process  $S_k, k \in \mathbb{Z}$  is a discrete time series, consisting of spread values subsampled every  $\Delta = 30s$  (as shown below, we explore the effects of varying this sub-sampling interval which plays also the role of the time-horizon between 3 seconds and 30 seconds) :

$$\begin{aligned}\lambda_k &= c + \alpha S'_{k-1} + \beta \lambda_{k-1} \\ S'_k | \mathcal{F}_{k-1} &\sim \mathcal{DP}(\lambda_k, \gamma)\end{aligned}\tag{13}$$

where  $S'_k = S_k - 1 \in \mathbb{N}$ , and  $\mathcal{DP}(\lambda_k, \gamma)$  stands for the Double Poisson distribution defined by

$$\mathbb{P}(S'_k = n | \lambda_k, \gamma) = c(\gamma, \lambda_k) \gamma^{1/2} e^{-\gamma \lambda_k} \left( \frac{e^{-n} n^n}{n!} \right) \left( \frac{e \lambda_k}{n} \right)^{\gamma n}$$

Under this model,  $\mathbb{E}[S'_k | \mathcal{F}_{k-1}] = \lambda_k$ .

As shown in [Groß-Klußmann and Hautsch, 2013], the log likelihood function of ACDP model reads:

$$\log \mathcal{L}(c, \alpha, \beta, \gamma | S'_{[1:N]}) = \sum_{k=1}^T \left( \frac{1}{2} \log(\gamma) - \gamma \lambda_k + S'_k (\log S'_k - 1) - \log(S'_k!) + \gamma S'_k \left( 1 + \log\left(\frac{\lambda_k}{S'_k}\right) \right) \right)$$

where  $\lambda_t = (1 - \beta B)^{-1}(c + \alpha B(S'_t))$  with  $B(S'_t) = S'_{t-1}$  being the backshift operator which gives, when  $\beta < 1$ :

$$\lambda_t = \sum_{i=0}^{\infty} \beta^i B^i(c + \alpha B(S'_t))$$

In practice, one estimates  $\lambda_t$  based on a truncation of the infinite sum, *i.e.*,  $\lambda_t = \sum_{i=0}^N \beta^i B^i(c + \alpha B(S'_t))$ , where  $N$  is an hyper parameter of the method. In this work, we set  $N$  to be 60. In fact, after experimenting with different values of  $N$ , we found that the results remain consistent as long as  $N$  is greater than 10.

**Numerical results** Let us present the numerical results on the relative performances of SDSH and ACDP based methods. We are going to compare three different predictors for time-horizons varying from  $\Delta = 3s$  up to  $\Delta = 30s$ .

- **SDSH predictor :**

- For each stock, the SDSH model is calibrated on training data which consists of 30-day spread dynamics within a 2-hour window each day (from 10am to 12pm) for avoiding strong seasonal effects.
- No re-estimation of the model parameters is made along running the test
- At each time, forecasting is made using the previous 1 minute data following Eqs (11) and (12)

• **ACDP predictor :**

- For each stock, the ACDP model is calibrated using a time rolling window of 1-hour of spread data subsampled every  $\Delta$  seconds.
- Parameters are reestimated every 10 minutes to ensure that the predictions remain up-to-date.
- The model employs a one-step ahead prediction strategy using the most recent estimated model for forecasting

- **Last predictor :** A simple benchmark predictor that consists in considering a that  $S_t$  is a martingale, *i.e.*, in taking the last observable value of the spread  $\hat{S}_{t_0+\Delta} = S_{t_0}$  as the best prediction.

All methods are evaluated over a test period lasting 50 consecutive days, following the initial 30-day training period for the SDSH model. The evaluation takes place specifically from 11am to 12pm every day. This time-frame is chosen to accommodate the ACDP method, as it requires a minimum of one hour to calibrate the model before generating predictions. Therefore, we cannot make predictions before 11am.

$\Delta$	3s	6s	12s	30s	$\Delta$	3s	6s	12s	30s
Last	0.408	0.587	0.784	1.082	Last	0.833	1.177	1.487	1.818
ACDP	0.514	0.520	0.565	0.808	ACDP	0.737	<b>0.851</b>	0.971	1.320
SDSH	<b>0.363</b>	<b>0.478</b>	<b>0.561</b>	<b>0.648</b>	SDSH	<b>0.692</b>	0.865	<b>0.964</b>	<b>1.065</b>

(a) AXA					(b) BNP				
$\Delta$	3s	6s	12s	30s	$\Delta$	3s	6s	12s	30s
Last	0.388	0.609	0.904	1.340	Last	0.370	0.421	0.445	0.457
ACDP	0.508	0.609	<b>0.744</b>	<b>1.031</b>	ACDP	0.283	0.258	0.256	0.267
SDSH	<b>0.361</b>	<b>0.543</b>	0.766	1.081	SDSH	<b>0.230</b>	<b>0.240</b>	<b>0.244</b>	<b>0.245</b>

(c) NOKIA					(d) Cac40 Index Future				
$\Delta$	3s	6s	12s	30s	$\Delta$	3s	6s	12s	30s
Last	0.388	0.609	0.904	1.340	Last	0.370	0.421	0.445	0.457
ACDP	0.508	0.609	<b>0.744</b>	<b>1.031</b>	ACDP	0.283	0.258	0.256	0.267
SDSH	<b>0.361</b>	<b>0.543</b>	0.766	1.081	SDSH	<b>0.230</b>	<b>0.240</b>	<b>0.244</b>	<b>0.245</b>

Table 3: Mean Square Error (MSE) of the 3 different predictors, Last, ACDP and SDSH for different time sub-samplings  $\Delta$  (which plays also the role of the time-horizon).

We evaluate these two predictors on three stocks (AXA, BNP Paribas and Nokia) as well as the Cac40 index future. The performance comparison is presented in Table 3.

As table 3 shows, the Last predictor is always worse than the SDSH predictor though it outperforms the ACDP predictor sometimes at the highest frequency (i.e.,  $\Delta = 3s$ , for AXA and NOKIA). Moreover the SDSH predictor outperforms most of the time the ACDP predictor (and systematically for the highest frequency  $\Delta = 3s$ ). These results are very encouraging as far as the SDSH prediction performances are concerned. A Detailed comparison with several state of the art predictors and for a wider range of time horizons will be addressed in a forthcoming work.

## 6 Conclusion

In this paper, we introduced a State Dependent Hawkes process (SDSH) for modelling bid-ask spread fluctuations, which generalizes the spread models presented in [Zheng et al., 2014] and [Fosset et al., 2020a]. Our model is a 2K-variate Hawkes process which can accommodate different jump sizes (ranging from 1 to K). In order to account for the current spread value  $S_t$ , we introduced a spread-dependent term  $f^e(S_t)$  (where  $e$  denotes an event type) and multiplied the classical Hawkes intensity by this term. We chose to use the sum of exponential kernels to benefit from the Markovian properties of the model. Notably, we demonstrated the ergodicity property in a particular case, indicating that the spread process converges to a stationary distribution over time.

Then we calibrated our SDSH model using high-frequency data obtained from Cac40 Euronext Market, including three stocks (AXA, BNP, Nokia) and the Cac40 Future index. We examined the estimated spread-dependent term  $f$ , as well as kernel functions to better understand how they affect the spread dynamics. Our analysis revealed that the estimated  $f^e(\cdot)$  is decreasing when  $e$  is an event which increased the spread, while for at least one downward event  $e'$ ,  $f^{e'}(\cdot)$  is increasing. Such  $f^e$  is able to press the spread down when its value is high by exciting more downward events. In terms of kernel functions, our estimation results showed that most of them tend to decrease very slowly, resembling a power-law kernel function.

We studied the ability of this model to capture various spread statistics. We found that our model very successfully replicates the spread distributions, measured by both calendar time and event time. We also observed that the model accurately reproduces other important statistical features, including the distributions

of inter-event times, spread autocorrelations as well as spread increments autocovariance.

Finally we demonstrated the effectiveness of the SDSH model in predicting the spread across different sample window sizes. Our results suggest that the SDSH model is a reliable and robust choice for predicting the spread.

As part of future work, we plan to expand our spread model to higher dimension, for example by incorporating bid and ask processes.

## Acknowledgements

We thank Euronext for making their data available to us. This research is partially supported by the Agence Nationale de la Recherche as part of the “Investissements d’avenir” program (reference ANR-19-P3IA-0001; PRAIRIE 3IA Institute).

## References

- [Abergel and Jedidi, 2013] Abergel, F. and Jedidi, A. (2013). A mathematical approach to order book modeling. *International Journal of Theoretical and Applied Finance*, 16(05):1350025.
- [Bacry et al., 2017] Bacry, E., Bompain, M., Gaïffas, S., and Poulsen, S. (2017). Tick: a python library for statistical learning, with a particular emphasis on time-dependent modelling. *arXiv preprint arXiv:1707.03003*.
- [Bacry et al., 2013] Bacry, E., Delattre, S., Hoffmann, M., and Muzy, J. (2013). Modelling microstructure noise with mutually exciting point processes. *Quantitative Finance*, 13:65–77.
- [Bacry et al., 2016] Bacry, E., Jaisson, T., and Muzy, J.-F. (2016). Estimation of slowly decreasing Hawkes kernels: application to high-frequency order book dynamics. *Quantitative Finance*, 16(8):1179–1201.
- [Bacry et al., 2015] Bacry, E., Mastromatteo, I., and Muzy, J.-F. (2015). Hawkes processes in finance. *Market Microstructure and Liquidity*, 01(01):1550005.
- [Bessembinder, 1994] Bessembinder, H. (1994). Bid-ask spreads in the interbank foreign exchange markets. *Journal of Financial Economics*, 35(3):317–348.
- [Bochud and Challet, 2007] Bochud, T. and Challet, D. (2007). Optimal approximations of power laws with exponentials: application to volatility models with long memory. *Quantitative Finance*, 7(6):585–589.
- [Bouchaud et al., 2018] Bouchaud, J.-P., Bonart, J., Donier, J., and Gould, M. (2018). *Trades, quotes and prices: financial markets under the microscope*. Cambridge University Press.
- [Bouchaud et al., 2009] Bouchaud, J.-P., Farmer, J. D., and Lillo, F. (2009). How markets slowly digest changes in supply and demand. In *Handbook of financial markets: dynamics and evolution*, pages 57–160. Elsevier.
- [Bouchaud et al., 2002] Bouchaud, J.-P., Mézard, M., and Potters, M. (2002). Statistical properties of stock order books: empirical results and models. *Quantitative finance*, 2(4):251.
- [Bowser, 2007] Bowser, C. (2007). Modelling security market events in continuous time: Intensity based point process models. *Journal of Econometrics*, 141(2):876–912.
- [Cattivelli and Pirino, 2019] Cattivelli, L. and Pirino, D. (2019). A sharp model of bid–ask spread forecasts. *International Journal of Forecasting*, 35(4):1211–1225.
- [Cont et al., 2010] Cont, R., Stoikov, S., and Talreja, R. (2010). A stochastic model for order book dynamics. *Operations Research*, 58(3):549–563.

- [Daniels et al., 2003] Daniels, M. G., Farmer, J. D., Gillemot, L., Iori, G., and Smith, E. (2003). Quantitative model of price diffusion and market friction based on trading as a mechanistic random process. *Physical review letters*, 90(10):108102.
- [Dayri and Rosenbaum, 2015] Dayri, K. and Rosenbaum, M. (2015). Large tick assets: implicit spread and optimal tick size. *Market Microstructure and Liquidity*, 1(01):1550003.
- [Díaz and Escribano, 2020] Díaz, A. and Escribano, A. (2020). Measuring the multi-faceted dimension of liquidity in financial markets: A literature review. *Research in International Business and Finance*, 51:101079.
- [Down et al., 1995] Down, D., Meyn, S. P., and Tweedie, R. L. (1995). Exponential and uniform ergodicity of markov processes. *The Annals of Probability*, 23(4):1671–1691.
- [Fall et al., 2021] Fall, M., Louhichi, W., and Viviani, J. L. (2021). Forecasting the intra-day effective bid ask spread by combining density forecasts. *Applied Economics*, 53(50):5772–5792.
- [Fong et al., 2017] Fong, K. Y., Holden, C. W., and Trzcinka, C. A. (2017). What are the best liquidity proxies for global research? *Review of Finance*, 21(4):1355–1401.
- [Fosset et al., 2020a] Fosset, A., Bouchaud, J.-P., and Benzaquen, M. (2020a). Endogenous liquidity crises. *Journal of Statistical Mechanics: Theory and Experiment*, 2020(6):063401.
- [Fosset et al., 2020b] Fosset, A., Bouchaud, J.-P., and Benzaquen, M. (2020b). Non-parametric estimation of quadratic hawkes processes for order book events. *Available at SSRN 3599027*.
- [Foucault et al., 2005] Foucault, T., Kadan, O., and Kandel, E. (2005). Limit order book as a market for liquidity. *The review of financial studies*, 18(4):1171–1217.
- [Glosten and Harris, 1988] Glosten, L. R. and Harris, L. E. (1988). Estimating the components of the bid/ask spread. *Journal of financial Economics*, 21(1):123–142.
- [Glosten and Milgrom, 1985] Glosten, L. R. and Milgrom, P. R. (1985). Bid, ask and transaction prices in a specialist market with heterogeneously informed traders. *Journal of financial economics*, 14(1):71–100.
- [Goyenko et al., 2009] Goyenko, R. Y., Holden, C. W., and Trzcinka, C. A. (2009). Do liquidity measures measure liquidity? *Journal of financial Economics*, 92(2):153–181.
- [Groß-Klußmann and Hautsch, 2013] Groß-Klußmann, A. and Hautsch, N. (2013). Predicting bid–ask spreads using long-memory autoregressive conditional poisson models. *Journal of Forecasting*, 32(8):724–742.
- [Hardiman et al., 2013] Hardiman, S. J., Bercot, N., and Bouchaud, J.-P. (2013). Critical reflexivity in financial markets: a hawkes process analysis. *Eur. Phys. J. B*, 86:442.
- [Hawkes, 1971] Hawkes, A. G. (1971). Point spectra of some mutually exciting point processes. *Journal of the Royal Statistical Society: Series B (Methodological)*, 33(3):438–443.
- [Huang and Stoll, 1997] Huang, R. D. and Stoll, H. R. (1997). The components of the bid-ask spread: A general approach. *The Review of Financial Studies*, 10(4):995–1034.
- [Large, 2007] Large, J. (2007). Measuring the resiliency of an electronic limit order book. *Journal of Financial Markets*, 10(1):1–25.
- [Lee and Seo, 2022] Lee, K. and Seo, B. K. (2022). Modeling Bid and Ask Price Dynamics with an Extended Hawkes Process and Its Empirical Applications for High-Frequency Stock Market Data. *Journal of Financial Econometrics*. nbab029.
- [Lewis and Shedler, 1979] Lewis, P. W. and Shedler, G. S. (1979). Simulation of nonhomogeneous poisson processes by thinning. *Naval research logistics quarterly*, 26(3):403–413.
- [Mike and Farmer, 2008] Mike, S. and Farmer, J. D. (2008). An empirical behavioral model of liquidity and volatility. *Journal of Economic Dynamics and Control*, 32(1):200–234.
- [Morariu-Patrichi and Pakkanen, 2018] Morariu-Patrichi, M. and Pakkanen, M. S. (2018). State-dependent hawkes processes and their application to limit order book modelling. *arXiv preprint arXiv:1809.08060*.

- [Muni Toke and Pomponio, 2012] Muni Toke, I. and Pomponio, F. (2012). Modelling trades-through in a limit order book using hawkes processes. *Economics - The Open-Access, Open-Assessment E-Journal*, 6:1–23.
- [Muni Toke and Yoshida, 2017] Muni Toke, I. and Yoshida, N. (2017). Modelling intensities of order flows in a limit order book. *Quantitative Finance*, 17(5):683–701.
- [Ogata, 1981] Ogata, Y. (1981). On lewis’ simulation method for point processes. *IEEE transactions on information theory*, 27(1):23–31.
- [Plerou et al., 2005] Plerou, V., Gopikrishnan, P., and Stanley, H. E. (2005). Quantifying fluctuations in market liquidity: Analysis of the bid-ask spread. *Physical Review E*, 71(4):046131.
- [Ponzi et al., 2006] Ponzi, A., Lillo, F., and Mantegna, R. N. (2006). Market reaction to temporary liquidity crises and the permanent market impact. *arXiv preprint physics/0608032*.
- [Rambaldi et al., 2017] Rambaldi, M., Bacry, E., and Lillo, F. (2017). The role of volume in order book dynamics: a multivariate hawkes process analysis. *Quantitative Finance*, 17(7):999–1020.
- [Roşu, 2009] Roşu, I. (2009). A dynamic model of the limit order book. *The Review of Financial Studies*, 22(11):4601–4641.
- [Smith et al., 2003] Smith, E., Farmer, J. D., Gillemot, L., and Krishnamurthy, S. (2003). Statistical theory of the continuous double auction. *Quantitative finance*, 3(6):481.
- [Stoll, 1989] Stoll, H. R. (1989). Inferring the components of the bid-ask spread: Theory and empirical tests. *the Journal of Finance*, 44(1):115–134.
- [Wu et al., 2019] Wu, P., Rambaldi, M., Muzy, J.-F., and Bacry, E. (2019). Queue-reactive hawkes models for the order flow. *arXiv e-prints*, pages arXiv–1901.
- [Wyart et al., 2008] Wyart, M., Bouchaud, J.-P., Kockelkoren, J., Potters, M., and Vettorazzo, M. (2008). Relation between bid–ask spread, impact and volatility in order-driven markets. *Quantitative finance*, 8(1):41–57.
- [Zawadowski et al., 2006] Zawadowski, Á. G., Andor, G., and Kertész, J. (2006). Short-term market reaction after extreme price changes of liquid stocks. *Quantitative Finance*, 6(4):283–295.
- [Zheng et al., 2014] Zheng, B., Roueff, F., and Abergel, F. (2014). Modelling bid and ask prices using constrained hawkes processes: Ergodicity and scaling limit. *SIAM Journal on Financial Mathematics*, 5(1):99–136.
- [Zumbach, 2004] Zumbach, G. (2004). How trading activity scales with company size in the ftse 100. *Quantitative finance*, 4(4):441–456.

## Appendices

### A Proof of V-uniform ergodicity

We restrict our model to the case where  $K = 1$  and  $L = 1$ . The model then writes

$$\lambda^e(t) = f^e(S_{t-})(\mu^e + \sum_{e' \in \mathcal{E}} \int_0^t \phi^{e,e'}(t-s) dS_s^{e'})$$

where  $\mathcal{E} = \{+1, -1\} =: \{+, -\}$  and  $\phi^{e,e'}(t) = \alpha^{e,e'} \beta e^{-\beta t}$

This section is devoted to the prove of the Proposition 2 of Section 2.3 that we replicate here :

**Proposition 3.** Let us consider the model given just above, assume that the following conditions are satisfied

$$(A) = \begin{cases} f^-(1) = 0 & (A_1) \\ f^-(S) \geq \gamma S \text{ for some } \gamma > 0 \text{ when } S \geq 2 & (A_2) \\ \sup_S \{f^+(S)\}(\alpha^{+,-} + \alpha^{+,+}) < 1 & (A_3) \end{cases}$$

then the process  $(S_t, X_t)$  is a  $V$ -uniformly ergodic Markov process.

**Remark 1.** It is worth noting that in this model, the last condition  $\sup_S \{f^+(S)\}(\alpha^{+,-} + \alpha^{+,+}) < 1$  is equivalent to  $(\alpha^{+,-} + \alpha^{+,+}) < 1$  and  $\sup_S \{f^+(S)\} \leq 1$ .

**Remark 2.** From now, we replace event  $+$  by 1 and  $-$  by 2. To avoid the ambiguity of notation, in the following part, we replace the superscripts by subscripts.

**Proposition 4.** Define  $X_{e,e'}(t) := \int_0^t \phi^{e,e'}(t-s) dN_s^{e'}$ . Then  $(X, S)$  is Markovian, where  $X = (X_{lm})_{l,m \in \{1,2\}}$ .

## Lyapunov function

As  $X_{lm}(t) = \int_0^t \alpha_{lm} e^{-\beta(t-s)} dN_s^m$ ,

$$dX_{lm}(t) = -\beta X_{lm}(t)dt + \alpha_{lm} dN_t^m$$

**Function**  $V_{lm}(X_{lm})$

$$V_{lm}(X_{lm}) = X_{lm}$$

The infinitesimal generator  $\mathcal{L}$  of  $X_{lm}$  on  $V_{lm}$

$$\begin{aligned} \mathcal{L}V_{lm}(X) &= \alpha_{lm} \lambda_m - \beta X_{lm} \\ &= -\beta X_{lm} + \alpha_{lm} f_m(S) \mu_m + \alpha_{lm} f_m(S) \left( \sum_n \beta X_{mn} \right) \\ &= -\beta X_{lm} + \alpha_{lm} \mu_m f_m(S) + \alpha_{lm} \beta f_m(S) (X_{m1} + X_{m2}) \end{aligned}$$

**Function**  $V_S(S)$

$$V_2(S) = S$$

As  $dS_t = dN_t^1 - dN_t^2$ , the infinitesimal generator  $\mathcal{L}$  of  $S$  on  $V_S$ :

$$\begin{aligned} \mathcal{L}V_2(S) &= \lambda_1 - \lambda_2 \\ &= f_1(S) \mu_1 + \beta f_1(S) X_{11} + \beta f_1(S) X_{12} - f_2(S) \mu_2 - \beta f_2(S) X_{21} - \beta f_2(S) X_{22} \end{aligned}$$

**Function V on  $(X, S)$**  Now we consider a function  $V$  on  $(X, S)$

$$V(X, S) = \sum_{l,m \in \{1,2\}} \eta_{lm} X_{lm} + \eta S$$

where  $\eta_{lm}, \eta > 0$ .

Then the infinitesimal generator  $\mathcal{L}$  of  $(X, S)$  on  $V$  is:

$$\begin{aligned} \mathcal{L}V(X, S) &= -\eta_{11} \beta X_{11} + \eta_{11} \alpha_{11} \mu_1 f_1(S) + \eta_{11} \alpha_{11} \beta f_1(S) (X_{11} + X_{12}) \\ &\quad -\eta_{12} \beta X_{12} + \eta_{12} \alpha_{12} \mu_2 f_2(S) + \eta_{12} \alpha_{12} \beta f_2(S) (X_{21} + X_{22}) \\ &\quad -\eta_{21} \beta X_{21} + \eta_{21} \alpha_{21} \mu_1 f_1(S) + \eta_{21} \alpha_{21} \beta f_1(S) (X_{11} + X_{12}) \\ &\quad -\eta_{22} \beta X_{22} + \eta_{22} \alpha_{22} \mu_2 f_2(S) + \eta_{22} \alpha_{22} \beta f_2(S) (X_{21} + X_{22}) \\ &\quad + \eta f_1(S) \mu_1 + \eta \beta f_1(S) X_{11} + \eta \beta f_1(S) X_{12} \\ &\quad - \eta f_2(S) \mu_2 - \eta \beta f_2(S) X_{21} - \eta \beta f_2(S) X_{22} \end{aligned}$$

Before giving the proof of Theorem 2, we should mention the following theorem. See Theorem 5.2 in [Down et al., 1995] and 2.5.2 in [Abergel and Jedidi, 2013].

**Theorem 1.** *For a  $\psi$ -irreducible, aperiodic Markov process  $X$ , if the following drift condition (D) holds, then  $X$  is  $V$ -uniformly ergodic.*

(D) For some  $\rho, b > 0$  and a coercive function  $V \geq 1$

$$\mathcal{L}V \leq -\rho V + b \quad (14)$$

*Proof of Theorem 2.* Suppose that we have already the following conditions:

$$(\mathcal{H}) = \begin{cases} \eta_{12}\alpha_{12} + \eta_{22}\alpha_{22} < \eta & (H_1) \\ \eta_{11}\alpha_{11} + \eta_{21}\alpha_{21} + \eta < \eta_{11} & (H_2) \\ \eta_{11}\alpha_{11} + \eta_{21}\alpha_{21} + \eta < \eta_{12} & (H_3) \end{cases}$$

To proceed, we will split  $\mathcal{L}V(X, S)$  into four distinct parts and show their individual upper bounds.

$$\mathcal{L}V(X, S) = I_1 + I_2 + I_3 + I_4$$

where

$$\begin{aligned} I_1 &= (1) + (2) \\ &= -\eta_{11}\beta X_{11} - \eta_{12}\beta X_{12} \\ &\quad + \eta_{11}\alpha_{11}\beta f_1(S)(X_{11} + X_{12}) + \eta_{21}\alpha_{21}\beta f_1(S)(X_{11} + X_{12}) + \eta\beta f_1(S)(X_{11} + X_{12}) \\ &< (-\eta_{11} + \eta_{11}\alpha_{11} + \eta_{21}\alpha_{21} + \eta)\beta X_{11} + (-\eta_{12} + \eta_{11}\alpha_{11} + \eta_{21}\alpha_{21} + \eta)\beta X_{12} \\ &< -\epsilon_1\beta X_{11} - \epsilon_2\beta X_{12} \end{aligned}$$

this last inequality is directly derived by conditions (H<sub>2</sub>) and (H<sub>3</sub>).

$$\begin{aligned} I_2 &= (3) + (4) \\ &= -\eta_{21}\beta X_{21} - \eta_{22}\beta X_{22} \\ &\quad + \eta_{12}\alpha_{12}\beta f_2(S)(X_{21} + X_{22}) + \eta_{22}\alpha_{22}\beta f_2(S)(X_{21} + X_{22}) - \eta\beta f_2(S)(X_{21} + X_{22}) \\ &= -\eta_{21}\beta X_{21} - \eta_{22}\beta X_{22} + (\eta_{12}\alpha_{12} + \eta_{22}\alpha_{22} - \eta)\beta f_2(S)(X_{21} + X_{22}) \\ &\stackrel{(H_1)}{<} -\eta_{21}\beta X_{21} - \eta_{22}\beta X_{22} \end{aligned}$$

Now for the other two terms  $I_3$  and  $I_4$ :

$$\begin{aligned} I_3 &= (5a) \\ &= \eta_{11}\alpha_{11}\mu_1 f_1(S) + \eta_{21}\alpha_{21}\mu_1 f_1(S) + \eta\mu_1 f_1(S) < \eta_{11}\alpha_{11}\mu_1 + \eta_{21}\alpha_{21}\mu_1 + \eta\mu_1 =: C_1 \end{aligned}$$

$$\begin{aligned} I_4 &= (5b) \\ &= \eta_{12}\alpha_{12}\mu_2 f_2(S) + \eta_{22}\alpha_{22}\mu_2 f_2(S) - \eta f_2(S)\mu_2 = (\eta_{12}\alpha_{12} + \eta_{22}\alpha_{22} - \eta)f_2(S)\mu_2 \\ &< -\epsilon_0\mu_2 f_2(S) \stackrel{(A_2)}{<} \epsilon_0\mu_2\gamma - \epsilon_0\mu_2\gamma S =: C_2 - \epsilon_0\mu_2\gamma S \end{aligned}$$

where

- $0 < \epsilon_0 < \eta - \eta_{12}\alpha_{12} - \eta_{22}\alpha_{22}$
- $0 < \epsilon_1 < \eta_{11} - (\eta_{11}\alpha_{11} + \eta_{21}\alpha_{21} + \eta)$
- $0 < \epsilon_2 < \eta_{12} - (\eta_{11}\alpha_{11} + \eta_{21}\alpha_{21} + \eta)$



Therefore

$$\begin{aligned}
\mathcal{L}V(X, S) &= I_1 + I_2 + I_3 + I_4 \\
&< -\epsilon_1\beta X_{11} - \epsilon_2\beta X_{12} - \eta_{21}\beta X_{21} - \eta_{22}\beta X_{22} + C_1 - \epsilon_0\mu_2 f_2(S) \\
&< -\epsilon_1\beta X_{11} - \epsilon_2\beta X_{12} - \eta_{21}\beta X_{21} - \eta_{22}\beta X_{22} + C_1 + C_2 - \epsilon_0\mu_2\gamma S \\
&< -\rho(\eta_{11}X_{11} + \eta_{12}X_{12} + \eta_{21}X_{21} + \eta_{22}X_{22} + \eta S) + C \\
&= -\rho V(X, S) + C
\end{aligned}$$

where  $\rho = \min\{\frac{\epsilon_1}{\eta_{11}}, \frac{\epsilon_2}{\eta_{12}}, 1, \frac{\epsilon_0\mu_2\gamma}{\eta}\}$ ,  $\beta > 0$  and  $C = C_1 + C_2$

Now we only need to find some  $\eta_{lm}, \eta > 0$  satisfying the hypothesis  $(\mathcal{H})$  to finish this proof.

As  $\alpha_{11} + \alpha_{12} < 1$ ,  $\frac{\alpha_{11}}{1 - \alpha_{12}} < 1 < \frac{1 - \alpha_{11}}{\alpha_{12}}$ . We note  $\delta = \frac{1}{2}(\frac{1 - \alpha_{11}}{\alpha_{12}} - 1)$ . Then the following values for  $\eta_{lm}, \eta$

$$\begin{cases} \eta_{11} = 1, \eta_{12} = \frac{1 - \alpha_{11}}{\alpha_{12}} - \delta > 1 = \eta^{11} \\ \eta_{21} = \delta \frac{\alpha_{12}}{4\alpha_{21}}, \eta_{22} = \delta \frac{\alpha_{12}}{4\alpha_{22}} \\ \eta = 1 - \alpha_{11} - \frac{1}{2}\delta\alpha_{12} \end{cases} \quad (15)$$

satisfy the condition  $(\mathcal{H})$ . □

**Remark 3.** For a more complicated version of our model :

$$\lambda^e(t) = f^e(S_{t-})(\mu^e + \sum_{e' \in \mathcal{E}} \int_0^t \phi^{e, e'}(t-s) dS_s^{e'})$$

where  $\mathcal{E} = \{+1, +2, -1, -2\}$ ,  $\phi^{e, e'}(t) = \alpha^{e, e'} \beta e^{-\beta t}$  (exponential kernels). Using the same proof, we can prove that under the following conditions  $(\mathcal{A}_1)$  and  $(\mathcal{H}_1)$ , the  $(X, S)$  is a  $V$ -uniformly ergodic Markov process.

$$(\mathcal{A}_1) = \begin{cases} f^{-1}(S) = 0 \text{ when } S = 1 \\ f^{-2}(S) = 0 \text{ when } S = 1, 2 \\ \max(f^{-1}(S), f^{-2}(S)) \geq \gamma S \text{ for some } \gamma > 0 \text{ when } S \geq 3 \\ f^{+1}(S), f^{+2}(S) \leq 1 \text{ for all } S \end{cases}$$

$$(\mathcal{H}_1) = \begin{cases} \sum_e \eta_{e, -1} \alpha^{e, -1} < \eta \\ \sum_e \eta_{e, -2} \alpha^{e, -2} < 2\eta \\ \sum_e \eta_{e, +1} \alpha^{e, +1} + \eta < \eta_{+1, e'}, \forall e' \in \mathcal{E} \\ \sum_e \eta_{e, +2} \alpha^{e, +2} + 2\eta < \eta_{+2, e'}, \forall e' \in \mathcal{E} \end{cases}$$

And the coercive function  $V$  is  $V(X, S) = \sum_{e, e' \in \mathcal{E}} \eta_{e, e'} X_{e, e'} + \eta S$

## B Log-likelihood function of spread model

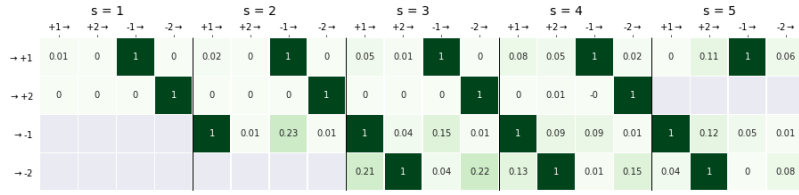
The log-likelihood function for the spread model is a function on  $\mu, \alpha$  and  $f$ . For brevity, we will only give the formula for the case where  $L = 1$  (only one decay). In order to distinguish from the above notations,

the log-likelihood function is denoted by  $\mathbb{L}$ .

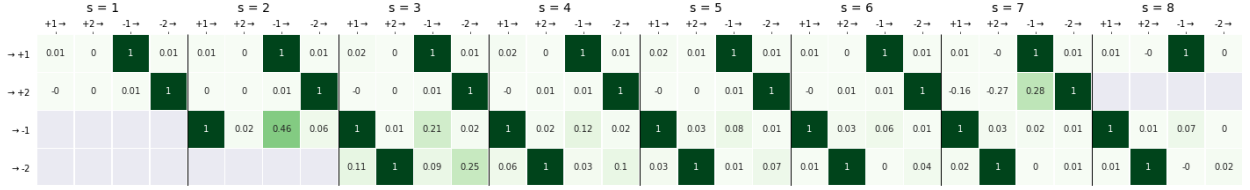
$$\begin{aligned}
\mathbb{L}(\alpha, \mu, f) &= \sum_{e=1}^{2K} \left( - \int_0^T \lambda^e(t) dt + \int_0^T \log \lambda^e(t) dS_t^e \right) \\
&= \sum_{e=1}^{2K} \sum_{k=1}^{S^e(T)} \log(\mu^e + \sum_{e'=1}^{2K} \alpha^{ee'} \beta \int_0^{t_k^e} e^{-\beta(t_k^e-s)} dS_s^j) + \sum_{e=1}^{2K} \sum_{k=1}^{S^e(T)} \log f^e(S_{t_k^e}) \\
&\quad - \sum_{e=1}^{2K} \int_0^T (\mu^e + \sum_{e'=1}^{2K} \alpha^{ee'} \beta \int_0^t e^{-\beta(t-s)} dS_s^{e'}) f^e(S_t) dt
\end{aligned} \tag{16}$$

where  $S^e(T)$  is the number of event  $e$  in  $[0, T]$ , and  $t_k^e$  is the timestamp where the  $k$ th event (type  $e$ ) occurs.

## C More numerical results



(a) BNP



(b) NOKIA

Figure 10: **Relative kernel integrated quantities**  $\tilde{I}_{s,e}(e')$  for (a)BNP and (b) NOKIA. For each stock, for each value of  $s$ , an image is displayed showing  $\tilde{I}_{s,e}(e')$  (defined by (8)) as a function of  $e$  (vertical axis) and  $e'$  (horizontal axis).

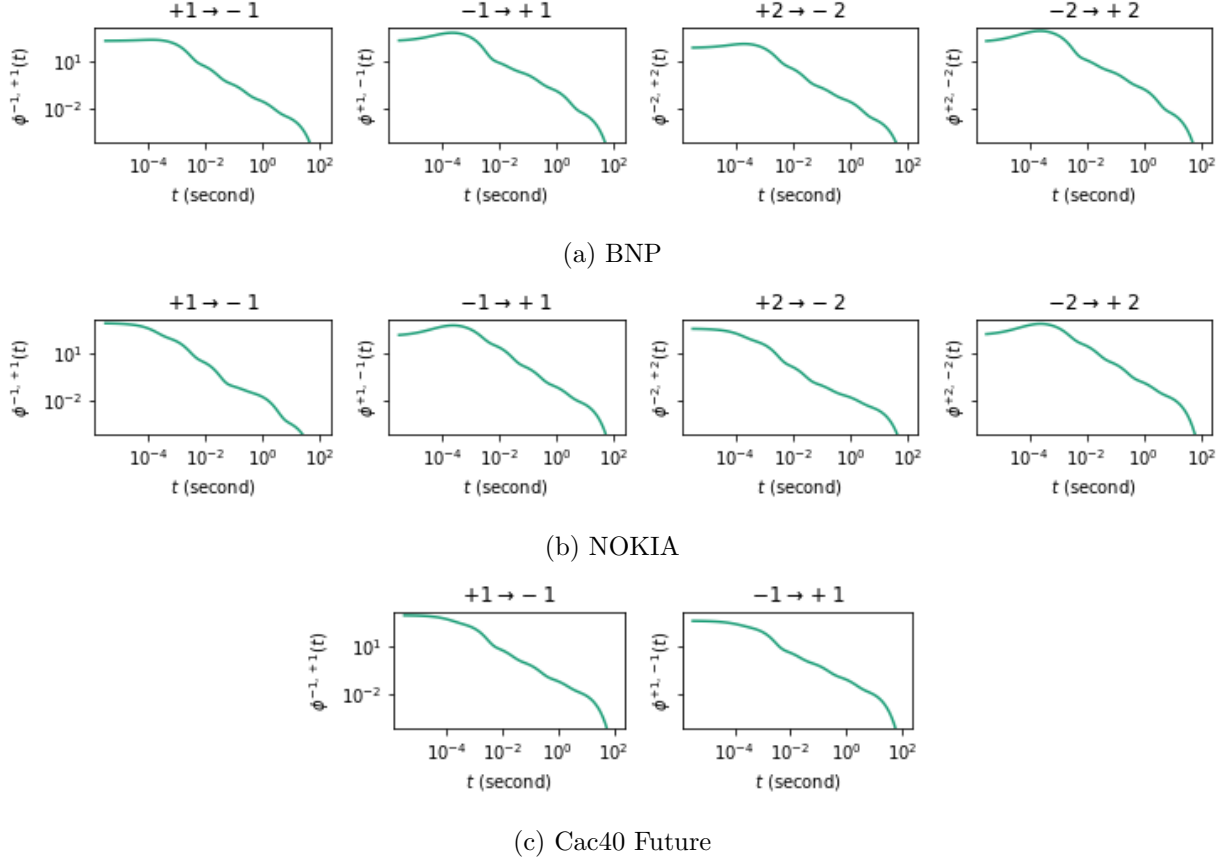
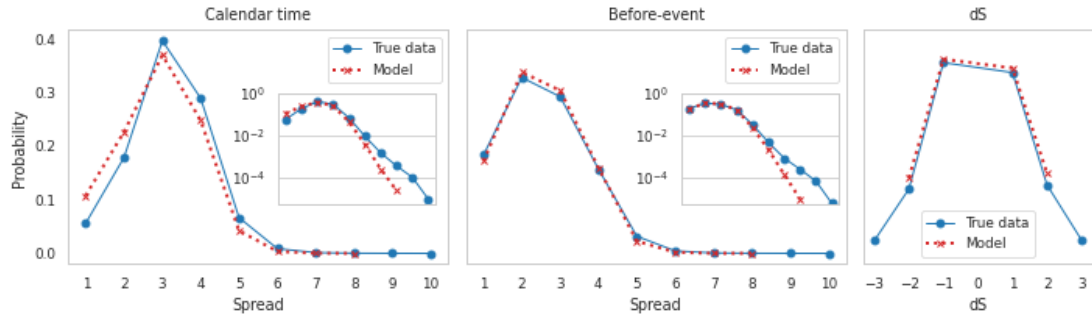
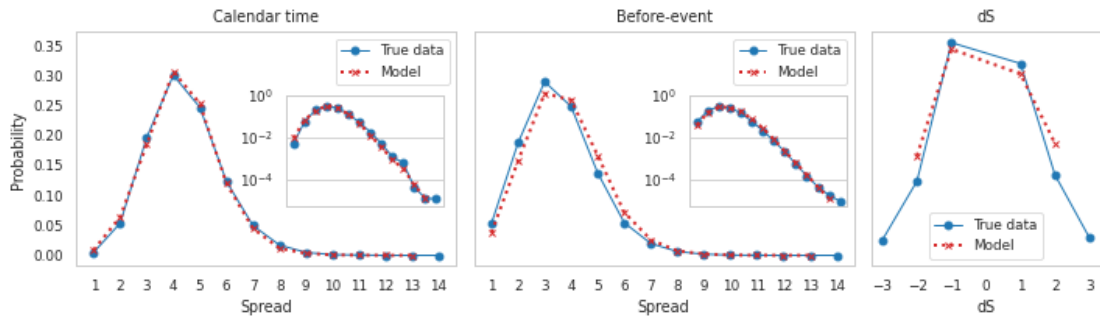


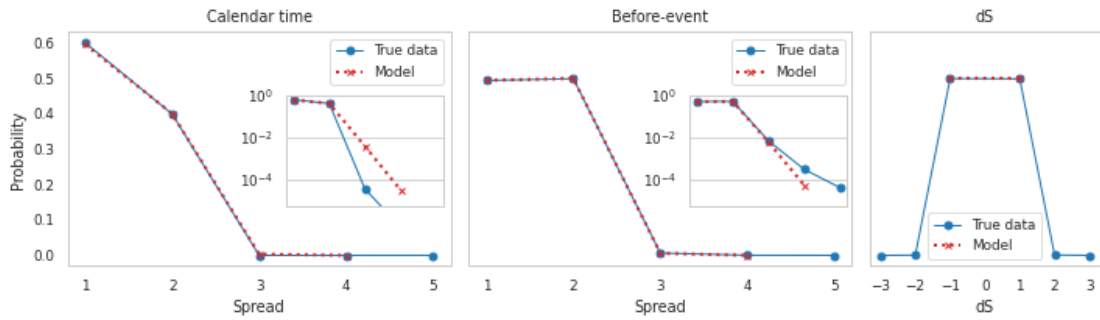
Figure 11: **Hawkes kernel shapes** for (a) BNP, (b) NOKIA, and (c) CAC40 Future. In this figure for each asset we present four contrarian Hawkes kernels (i.e., with  $e$  and  $e'$  with different signs (two contrarian Hawkes kernels for CAC40 Future) . Each kernel  $\phi^{e,e'}$  (labelled  $e' \rightarrow e$  on the figure with  $e, e' \in \mathcal{E}$ ) represents the influence of the past jumps of size  $e'$  on the occurrence probability of a future jumps of size  $e$ . Each kernel is represented by a sum of  $L = 6$  exponentials, i.e.,  $\phi^{e,e'}(t)$ , where  $\phi^{e,e'}(t) = \sum_l^L \alpha_l^{e,e'} \beta_l e^{-\beta_l t}$ , where  $\beta_l = \frac{1}{\tau_l}$  with  $\tau_l$  taken in  $\{10^{-4}s, 10^{-3}s, \dots, 10^1s\}$  All the kernels are displayed on a log-log scale and show a power law behavior on a large range of scales (3, 4 or even 5 decades)



(a) BNP

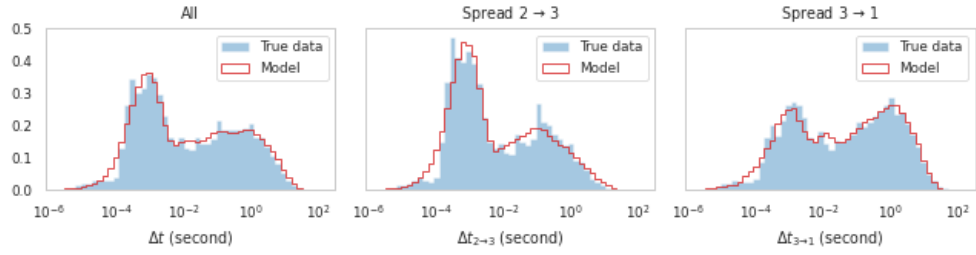


(b) NOKIA

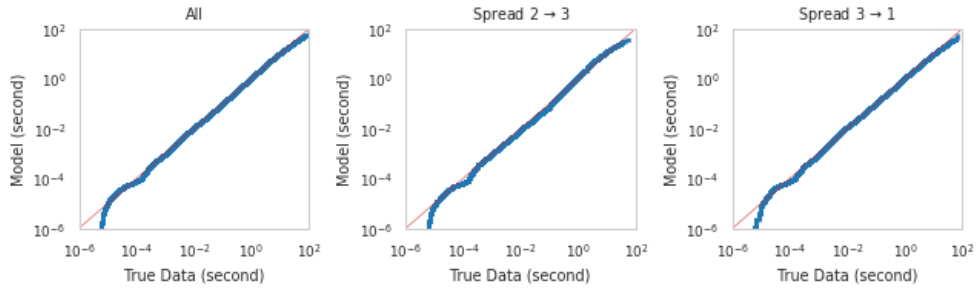


(c) Cac40 Future

Figure 12: **Spread distributions**, comparison between true data and the the data obtained through simulation of (a) AXA, (b) BNP, (c) NOKIA, (d) CAC40 Future. The left-hand figures are the Calendar time distributions, the middle figures are the event time distributions, and the right-hand figures are the distributions of spread jumps size.

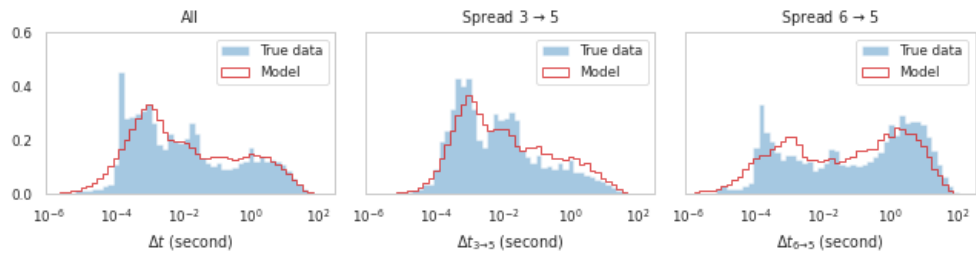


(a)

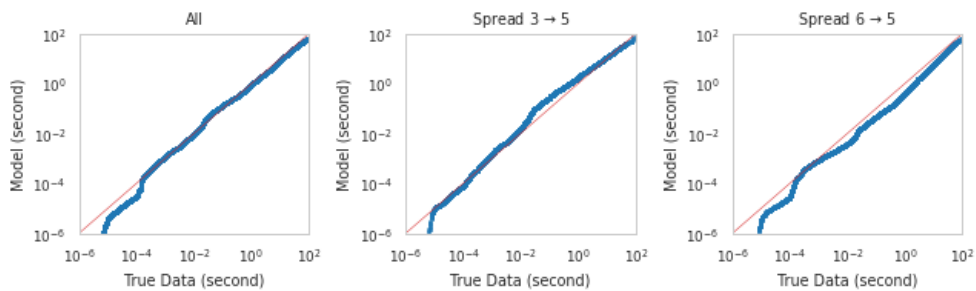


(b)

Figure 13: **BNP Inter-event time distributions.** (a) Compare empirical inter-event-time distribution with simulated inter-event-time distribution. The x-axis is on log scale. (b) Log-log qq-plot of empirical inter-event-times (x-axis) *vs.* simulated inter-event-times by model (y-axis).



(a)



(b)

Figure 14: **NOKIA Inter-event time distributions.** (a) Compare empirical inter-event-time distribution with simulated inter-event-time distribution. The x-axis is on log scale. (b) Log-log qq-plot of empirical inter-event-times (x-axis) *vs.* simulated inter-event-times by model (y-axis).

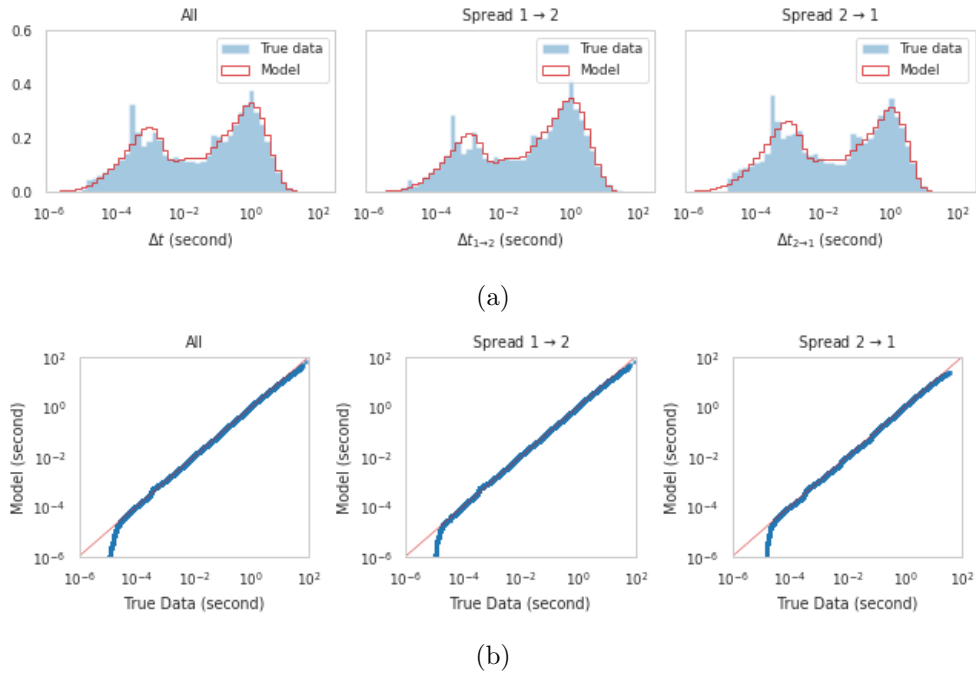


Figure 15: **Cac40 index Future Inter-event time distributions** (a) Compare empirical inter-event-time distribution with simulated inter-event-time distribution. The x-axis is on log scale. (b) Log-log qq-plot of empirical inter-event-times (x-axis) *vs.* simulated inter-event-times by model (y-axis).

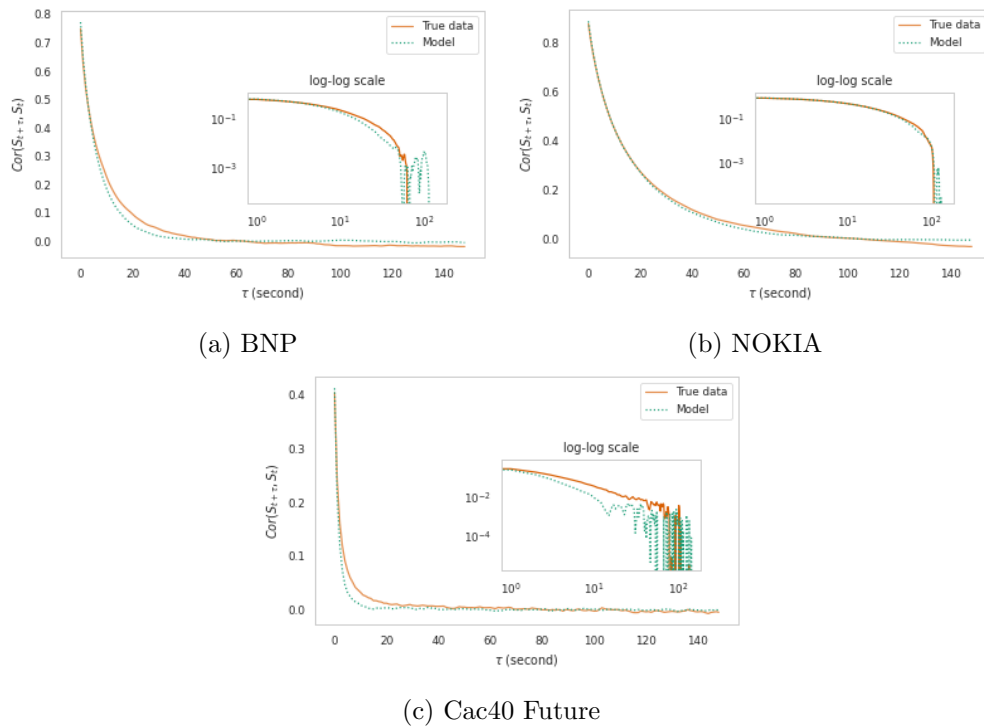


Figure 16: **Spread autocorrelation** for (a) BNP, (b) Nokia, (c) Cac40 index Future. True data versus model-simulated data. Each plot corresponds to a different asset. Quadratic variations were used for estimation. Eight 15min time-slots (between 10am and 12pm) were used everyday for true data in order to avoid intraday seasonal effects. 2 hours slots were used for model-simulated data.

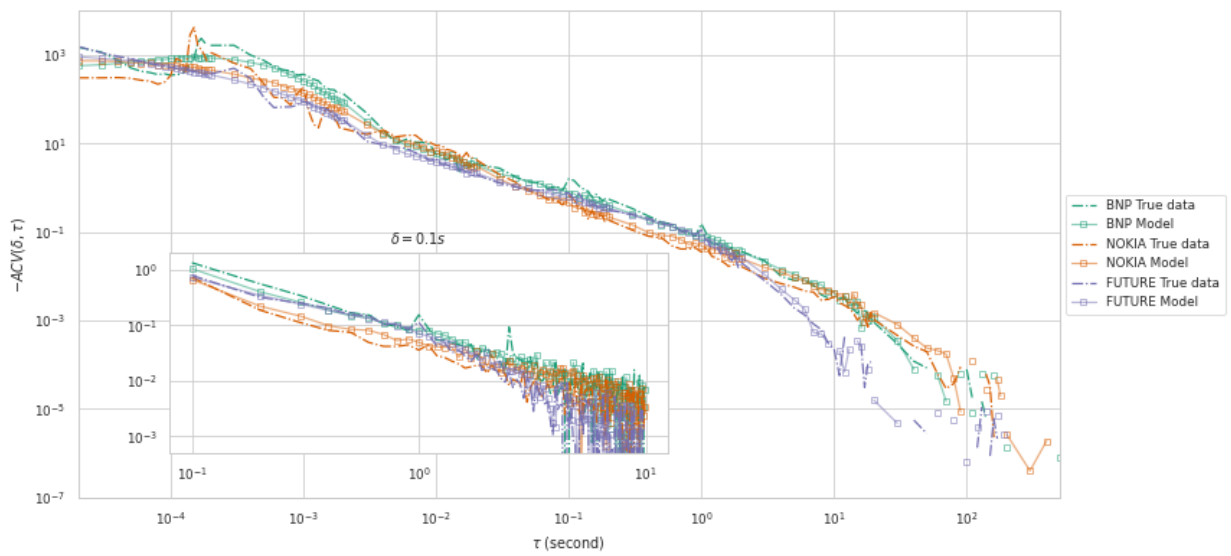


Figure 17: **Autocovariance of spread increments.** The  $-ACV(\delta, \tau)$  function for the different assets. For each asset the curves that are displayed (in the main plot and in the inset) follow the same protocol as the one of Fig. 9